Accepted Manuscript

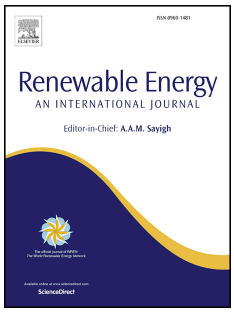

On the take-off of airborne wind energy systems based on rigid wings

L. Fagiano, S. Schnez

PII: S0960-1481(17)30101-5

DOI: 10.1016/j.renene.2017.02.023

Reference: RENE 8530

To appear in: *Renewable Energy*

Received Date: 15 February 2016

Revised Date: 7 February 2017

Accepted Date: 8 February 2017

Please cite this article as: Fagiano L, Schnez S, On the take-off of airborne wind energy systems based on rigid wings, *Renewable Energy* (2017), doi: 10.1016/j.renene.2017.02.023.

On the Take-off of Airborne Wind Energy Systems Based on Rigid Wings

L. Fagiano[a,b,1], S. Schnez[b,1]

[a]*Politecnico di Milano, Dipartimento di Elettronica, Informazione e Bioingegneria*
Piazza Leonardo da Vinci 32, 20133 Milano, Italy
[b]*ABB Switzerland Ltd, Corporate Research*
Segelhofstrasse 1K, CH - 5405 Baden-Dättwil, Switzerland

Abstract

The problem of launching a tethered rigid aircraft for airborne wind energy generation is investigated. Exploiting well-assessed physical principles, an analysis of four different take-off approaches is carried out. The approaches are then compared on the basis of quantitative and qualitative criteria introduced to assess their technical and economic viability. In particular, the additional power required by the take-off functionality is computed and related to the peak mechanical power generated by the system. Moreover, the additionally required on-board mass is estimated, which impacts the cut-in wind speed of the generator. Finally, the approximate ground area required for take-off is also determined. After the theoretical comparison, a deeper study of the concept that is deemed the most viable one, i.e. a linear take-off maneuver combined with on-board propellers, is performed by means of numerical simulations. The simulation results are used to refine the initial analysis and further confirm the viability of the approach.

Keywords: airborne wind energy, renewable energy, wind energy, mechatronic systems, tethered aircraft, autonomous take-off

1. Introduction

The term airborne wind energy (AWE) refers to a class of wind power generators that exploit tethered aircrafts to convert wind energy into electricity [1, 20]. The benefits of AWE systems, compared to traditional wind turbines, are essentially two: lower construction and installation costs and the possibility to reach higher altitudes, where faster and steadier winds blow. According to the current estimates, the combination of these two benefits should render AWE systems competitive with the established energy sources, including fossil fuels [21], in terms of both cost of energy and land occupation. The first papers and patents concerned with AWE appeared in the late 1970s (see e.g. [39, 36]), yet only in recent years a significant and growing research effort has been undertaken by both small companies and universities to develop such concepts via theoretical, numerical and experimental methods [1]. AWE is still at an early development stage and no commercial system exists. However, a relatively well-established set of few different approaches has emerged, while other, less promising ideas have been abandoned.

Today, AWE systems can be classified by the way the lift force that keeps the aircraft airborne is generated – either aerodynamic lift [28, 41, 44, 8, 42, 35], or aerostatic lift [45] – and by the placement of the electrical generators – either on-board of the aircraft [35, 45] or on the ground [28, 41, 8, 44, 42]. Among the systems that exploit aerodynamic lift and generators on ground, a further distinction can be made between concepts that rely on rigid wings [42], similar to gliders, and concepts that employ flexible wings, like power kites [28, 41, 44, 8]. Small-scale prototypes (10-50 kW of rated power) of all the mentioned concepts have been realized and successfully tested to demonstrate their power generation functionalities. Moreover, scientific contributions concerned with several different technical aspects, like the theoretical power yield [36, 4, 5], aerodynamics [10, 11, 9, 17, 34] and controls [31, 12, 6, 15, 23, 18, 27, 47, 14, 48]

Email addresses: lorenzo.fagiano@polimi.it (L. Fagiano), stephan.schnez@ch.abb.com (S. Schnez)
[1]Both authors contributed equally to this publication.

but also resource assessment [3, 2], economics [21, 49], prototype design [19] and power conversion [43], have recently appeared.

Despite the steady and promising development of the field, several relevant aspects still need to be addressed in order to ultimately prove the technical and economic feasibility of the idea. One of such aspects is the take-off of the aircraft, particularly for concepts that employ rigid wings and ground generation. In fact, while systems with on-board generation [35, 45], as well as kite-based systems with ground generation [28] are able to take off autonomously from a compact ground area, the same functionality for AWE systems with rigid wings and ground-level generators has not been achieved yet. There is evidence of autonomous take-off of this class of generators [33]; however by using a winch launch that requires a significant space in all directions in order to adapt to the wind conditions during take-off. As a consequence, one of the main advantages of AWE systems, i.e. the possibility of being installed in a large variety of locations at low costs, might be lost due to the need of a large area of land suitable for the take-off. So far, this issue has been addressed only to a limited extent within the scientific community. In Ref. [46], a rotational take-off is studied and simulated; however the focus is on the control and optimization aspects of this approach, rather than on its economic viability and the comparison with other possible methods. In Ref. [7], an analysis of several approaches is first carried out, considering different performance criteria, and three alternatives are deemed the most promising: buoyant systems, linear ground acceleration plus on-board propellers, and rotational take-off.

In order to address this important problem, we present here an analysis of four candidate approaches to realize the take-off of a rigid tethered aircraft with ground-based generation. More specifically, we compare a winch launch without on-board propellers as implemented by Ampyx Power [42, 33], a vertical lift approach with on-board vertical-axis propellers, like the one employed by Makani Power [35], KiteMill [29] and TwingTec [37], a rotational take-off, like the one considered in Refs. [46, 7], and a linear take-off technique combined with on-board horizontal-axis propellers. The latter concept is apparently pursued by the company Ampyx Power as well [33]. The analysis is instrumental to carry out a comparison among the considered approaches, based on a series of performance criteria that we introduce in order to quantify their viability. In particular, the additional power required by the take-off functionality is computed and related to the peak mechanical power generated by the system. Moreover, the required additional on-board mass is estimated, which impacts the cut-in wind speed of the generator. Finally, the approximate ground area required by the take-off is also determined.

The analysis and the subsequent comparison represent the first main contribution that the present paper adds to the existing scientific literature. Then, we study in more depth the concept that is deemed the most viable, i.e. the linear take-off maneuver combined with on-board propellers. In particular, we derive a dynamical model of the system that includes realistic aerodynamic coefficients, as well as friction and inertia, and we use it to refine the initial analysis in terms of power required for take-off. Since the system is unstable in open-loop, we also develop the feedback control algorithms required to stabilize the take-off maneuver and carry out the numerical simulations. The simulations described here have been also employed to design the components of a small-scale prototype, which we used to test the linear take-off approach experimentally [26, 25, 24]. The obtained experimental results match well with the theoretical ones developed here.

The paper is organized as follows: section 2 provides more details on the considered type of AWE system, which are needed to formulate rigorously the considered problem, and a brief description of the considered take-off approaches. The performance criteria are introduced in section 2, too. Section 3 presents the analysis of the four take-off concepts using basic physical equations. The numerical simulation study is reported in section 4. Final conclusions are drawn in section 5, together with a discussion of future research developments.

2. Preliminaries and problem formulation

We first describe the system under consideration and introduce the physical equations that link the main lumped design parameters to the generated mechanical power. These equations can be employed in a first-approximation dimensioning phase of the AWE generator and are used here to compute one of our performance criteria. For the complete details and derivation of the equations, we refer to [36, 22, 20, 1].

2.1. Airborne wind energy systems based on rigid aircrafts and ground-level generation

The considered AWE system is composed of a rigid aircraft, a ground unit (GU), and a tether connecting them, as depicted in Figure 1. The aircraft is equipped with sensors, actuators and on-board intelligence to attain autonomous

flight and realize the flight patterns required to generate power, as well as with communication capabilities to exchange information with the GU and possibly with other systems and infrastructure nearby.

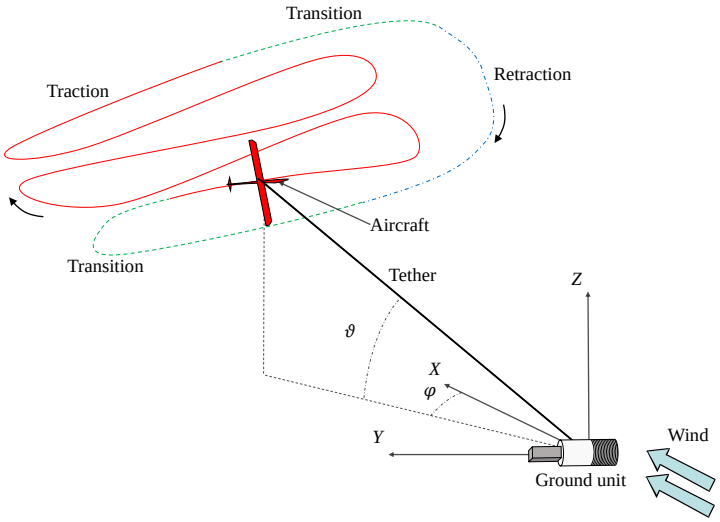

Figure 1: Sketch of the considered AWE generator and its working principle during power production. In the traction phase (red solid line) the aircraft is controlled to follow figure-of-eight patterns in crosswind conditions, and the tether is reeled out under large load from the drum installed in the GU. In the retraction phase (blue dash-dotted line), the aircraft is controlled to glide towards the ground station, and the tether is reeled-in under small load. Two transitions (green dashed lines) link the traction and retraction phases. The aircraft position with respect to the incoming wind can be defined by the elevation angle ϑ and the azimuth angle φ.

The GU consists of several subsystems, the main ones being a drum, around which the tether is coiled, an electric machine (generator/motor), linked to the drum through a mechanical transmission system, and the power electronic system to control the generator.

The described AWE system generates energy by means of a cyclic operating principle composed essentially of four phases: the power generation (or traction) phase, the retraction phase, and two transition phases linking them, shown in Figure 1. During the traction phase, the on-board control system steers the aircraft into figure-of-eight patterns under crosswind conditions. The generated aerodynamic forces exert a large traction load on the line, which is reeled-out from the drum. The electric machine exerts a torque on the drum in order to achieve a desired reel-out speed and to produce power. In particular, an aircraft with effective area A, aerodynamic lift and drag coefficients C_l and C_d, respectively, flying at a relative elevation ϑ and azimuth φ with respect to a wind flow of speed W (see Figure 1), exerts a traction load T on the tether approximately equal to [36, 22, 20]:

$$T(t) \simeq \tfrac{1}{2}\rho A \frac{C_l(t)^3}{C_{d,eq}(t)^2} \left(W(t)\cos(\varphi(t))\cos(\vartheta(t)) - \dot{l}(t)\right)^2 \tag{1}$$

where t is the continuous time variable, ρ is the air density, $C_{d,eq} \doteq C_d(t) + \frac{d_l\, l(t)\, C_{d,l}}{4A}$ is the equivalent drag coefficient (taking into account the drag of both the aircraft and the line), l is the length of the line, assumed straight, d_l its diameter, $C_{d,l}$ its drag coefficient, and $\dot{l} \doteq \frac{dl}{dt}$ is the tether reeling speed. For $\dot{l} > 0$, the line is reeled out from the drum, hence effectively decreasing the apparent wind speed parallel to the tether direction, given by $W\cos(\varphi)\cos(\vartheta)$. The tether force $T(t)$ multiplied with the reeling speed $\dot{l}(t)$ provides an estimate of the instantaneous mechanical power $P_m(t)$ generated during the traction phase:

$$P_m(t) \simeq T(t)\,\dot{l}(t). \tag{2}$$

The maximum generated power is achieved when the reeling speed is equal to 1/3 of the absolute wind speed projected along the line direction, i.e. $\dot{l} = \frac{1}{3} W \cos(\varphi)\cos(\vartheta)$, and ideally with $\varphi = \vartheta = 0$. In this case, the obtained mechanical power is:

$$P_m^*(t) \simeq \frac{2}{27}\rho A \cdot \frac{C_l(t)^3}{C_{d,eq}(t)^2} W(t)^3. \tag{3}$$

For the sake of estimating the generated power, the mass of the airborne components is irrelevant as a first approximation, since weight and apparent forces are significantly smaller than the force acting on the tether during the traction phase. On the other hand, this parameter clearly plays a crucial role when discussing take-off approaches. In order to evaluate a given take-off technique on a quantitative basis, the total mass of the aircraft m has to be linked to the system's capability in terms of force and power. Such a link is given by the so-called wing loading w_l, i.e. the ratio between m and the effective aerodynamic area A:

$$m = w_l A. \tag{4}$$

The wing loading increases in general with the expected peak mechanical power, since the latter is linked to the load values considered in the structural design of the aircraft. In fact, for given effective area and aerodynamic coefficients, a heavier structure (i.e. higher w_l) is required to sustain higher loads, since the cross-sections of the structural components and/or the density of the materials will increase. The total mass of the aircraft is the sum of m and of the additional mass Δm_i required for the take-off capability. This will be discussed further in section 2.3.

2.2. Take-off approaches

Here, we briefly describe the four take-off concepts under consideration.

Vertical take-off with rotors. In this approach, the aircraft is equipped with vertical-axis propellers which provide enough lift to take-off vertically. In the framework of ground-level generation, this approach is pursued by the company TwingTec [37]. In the AWE field, the company Makani Power owned by Google [38, 35] employs this approach for take-off and landing their system with on-board power generation.

Rotational take-off. This is the only proposal for rigid-wing systems which has been studied in the literature with numerical simulations in addition to static equations [7, 46]. In this approach, the hull of the aircraft is initially attached at the tip of a rotating arm. When the tangential speed of the arm is large enough, the aircraft takes off exploiting its aerodynamic lift and the tether is gradually extended out of the rotating arm until a certain altitude is reached. Then, the rotating arm is gradually slowed down while the aircraft transitions into power-generating mode. The company EnerKite [8] is implementing this concept for its AWE system.

Linear take-off with on-board propellers. In this approach the aircraft is accelerated on a rectilinear path up to take-off speed by an external source of power, for example the winch itself or a linear motion system. Horizontal-axis on-board propellers are then employed to sustain the forward speed during the climb to the operational altitude. This approach was briefly analyzed and deemed promising in Ref. [7], but without carrying out a deeper analysis by means of e.g. numerical simulations. The company Ampyx Power [42, 33] is developing a similar take-off concept as the one discussed here. Note that this approach is representative of a series of alternative technical solutions in addition to the one considered here, like for example Electromagnetic Aircraft Launch Systems (EMALS, [13]).

Winch launch. This is the approach currently implemented by Ampyx Power [42], and widely employed, outside the field of AWE, to launch gliders from the ground (with the important difference that in AWE systems the tether is never detached, differently from gliding applications). The aircraft is initially placed at a distance $l(0)$ from the GU in downwind direction, facing the wind. For the take-off, the winch reels the tether in at a speed $\dot{l}(t)$, which has to be large enough for the generated lift force to counteract the weight of the aircraft and start the ascend.

In the remainder of this paper, we will use the subscripts $_1$, $_2$, $_3$, and $_4$, respectively, for the vertical, rotational and linear take-off approaches and for the winch launch described above.

2.3. Performance criteria and problem formulation

A well-established metric to compare different electric power generation schemes on economic grounds is the levelized cost of electricity (LCOE). In our case, additional components or land occupation required to implement the take-off approach will increase upfront costs (and potentially maintenance costs) and will lead to an increase in the

LCOE of the AWE system, as compared to the same system without the take-off functionality. Hence, when comparing different take-off approaches, their impact on the LCOE should be assessed. However, the precise calculation of the LCOE is challenging for new power generation concepts like AWE systems.

Rather than the LCOE, we will therefore consider a series of other quantitative and qualitative criteria which are easier to evaluate based on the existing know-how of AWE generators, and which are related to the system's cost, complexity and required land occupation. If a specific take-off approach performs well according to these criteria, we can expect that the impact on the LCOE of the AWE system will be small.

The quantitative criteria are:

C1 The additional power installed on-board and on the ground, relative to the peak mechanical power of the system, required to carry out the take-off procedure:

$$\begin{aligned} \overline{P}_{g,i} &\simeq \eta_{P_g,i}\, P_m^* \\ \overline{P}_{ob,i} &\simeq \eta_{P_{ob},i}\, P_m^* \end{aligned} \tag{5}$$

where $\overline{P}_g$ and $\overline{P}_{ob}$ stand for the peak ground and on-board power, respectively, and $i = 1, 2, 3, 4$ refers to the four considered take-off approaches. The higher the values of $\eta_{P_g,i}$, $\eta_{P_{ob},i}$, the worse the approach.

C2 The additional on-board mass, relative to the aircraft's mass without the system required for the take-off:

$$\Delta m_i \simeq \eta_{m,i}\, m. \tag{6}$$

Although, as recalled in section 2.1, the mass does not impact the maximum power generation in a first approximation, it is an important parameter for the controllability and maneuverability of the system and for its capability to operate in a wide range of wind conditions [23]. Again, the higher $\eta_{m,i}$, the worse the approach.

C3 The ground area occupied by the take-off system, indicated with $A_{g,i}$:

$$A_{g,i} \simeq \underline{A}_{g,i} + \eta_{A_g,i}\, A, \tag{7}$$

where $\underline{A}_{g,i}$ is a fixed ground area occupied by the system independent from the wing's size. The higher $\underline{A}_{g,i}$, $\eta_{A_g,i}$, the worse the approach.

The qualitative criteria that we consider are:

C4 The complexity and cost of the apparatus that needs to be added to the system for the take-off functionality.

C5 The capability to take off under most wind conditions (including no wind).

The problem we will address in the next section is to carry out a comparison of the four considered approaches in light of criteria C1-C5. In particular, we will derive equations that allow to compute the quantitative criteria C1-C3, and we will assess the criteria C4-C5 on the basis of the knowledge on AWE systems available in the literature and of our own hands-on experience.

A viable and reliable landing procedure is of course required for any AWE concept to be successful. Hence, a sixth criterion could be whether a certain take-off concept can also be used "in reverse", i.e. for landing. However, landing is another challenge where approaches different from the take-off may be successful. We therefore refrain from including another criterion which qualitatively assesses the viability of a landing procedure.

3. Assessment of take-off concepts for rigid-wing AWE systems

In the following four sections we introduce the relevant assumptions and derive the governing equations of the considered take-off approaches. Quantitative results and the related discussion are presented in section 3.5.

3.1. Vertical take-off with rotors

According to the Actuator Disk Theory [30], the thrust through a disk with area A_{prop} is

$$T = \frac{1}{2}\rho A_{\text{prop}}\left(v_{\text{out}}^2 - v_{\text{in}}^2\right), \tag{8}$$

where the velocities are taken far in front and far behind the disk. The associated power is then

$$P_{ob,1} = \frac{1}{2}(v_{\text{out}} + v_{\text{in}})\,T. \tag{9}$$

In order to lift an object with vertical velocity v_{c} and mass m, the thrust must equal the weight, $T = mg$. By setting $v_{\text{in}} = v_{\text{c}}$ with v_{c} being the desired climb velocity, considering a conversion efficiency $\eta < 1$ between mechanical power at the shaft and fluid-dynamic power, and solving Eqs. (8) and (9) for $P_{ob,1}$, it then follows that the required take-off power is

$$P_{ob,1} = \frac{(m + \Delta m_1)g}{\eta}\left(\sqrt{\frac{(m + \Delta m_1)g}{2\rho A_{\text{prop}}} + \frac{v_{\text{c}}^2}{4}} + \frac{1}{2}v_{\text{c}}\right). \tag{10}$$

In our assessment, for the sake of computing $P_{ob,1}$, we will consider a wing with wingspan d and aspect ratio (i.e. wingspan divided by the chord) λ, and we will assume that the aircraft employs two propellers with a diameter equal to the chord length, i.e. d/λ. Thus, we have $A = d^2/\lambda$ and $A_{\text{prop}} = \dfrac{\pi\, d^2}{2\,\lambda^2}$. With regard to the additional on-board mass Δm_1, this is given mainly by the onboard batteries and electric motors that drive the propellers. The required battery mass is calculated from the energy density of lithium-polymer batteries E_{batt} and the required power $P_{ob,1}$, target altitude h and climb speed v_{c} (i.e. the climb duration is h/v_{c}). The power density of an electric motor is indicated by E_{mot}. The resulting equation for the additional on-board mass is:

$$\Delta m_1 = P_{ob,1}\left(\frac{h}{v_{\text{c}}\,E_{\text{batt}}} + \frac{1}{E_{\text{mot}}}\right) \tag{11}$$

We solve the system of Eqs. (10) and (11) to compute the required take-off power, in order to account also for the additional mass.

Finally, as regards the occupied ground area, we assume that the vertical take-off can be carried out with all possible angles between the wing and the nominal wind speed. Hence, we have

$$A_{g,1} = \frac{\pi d^2}{4} = \frac{\pi\lambda}{4}A \tag{12}$$

3.2. Rotational take-off

A schematic arrangement of the rotational take-off is shown in Figure 2: the hull of the aircraft is attached via the tether to the tip of a rotating arm with length R. The two angles γ_v and γ_h describe the orientation of the tether, assumed straight, with respect to the arm. The combination of lift force and centrifugal force due to the rotation leads to a reel out of the tether and the rise of the plane. If we assume that the angles γ_v and γ_h are constant during the rotational take-off, the sum of all forces perpendicular to the tether must cancel each other. Then, the required power to rotate the whole system (neglecting the drag of the rotating arm) is

$$P_{g,2} = RT_{\perp}\omega, \tag{13}$$

where

$$T_{\perp} = T \cdot \sin(\gamma_H)\cos(\gamma_V) \tag{14}$$

is the tether tension T projected onto the plane of the rotating arm and perpendicular to it and ω is the angular velocity of the system.

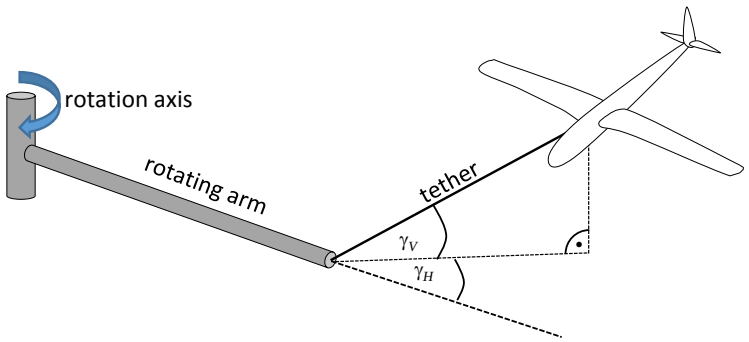

Figure 2: Sketch of an aircraft attached to a rotating arm via the tether during a rotational start. The azimuth of the plane is given by the angle γ_h; the angle γ_v denotes the angle between the tether and the plane of the rotating arm.

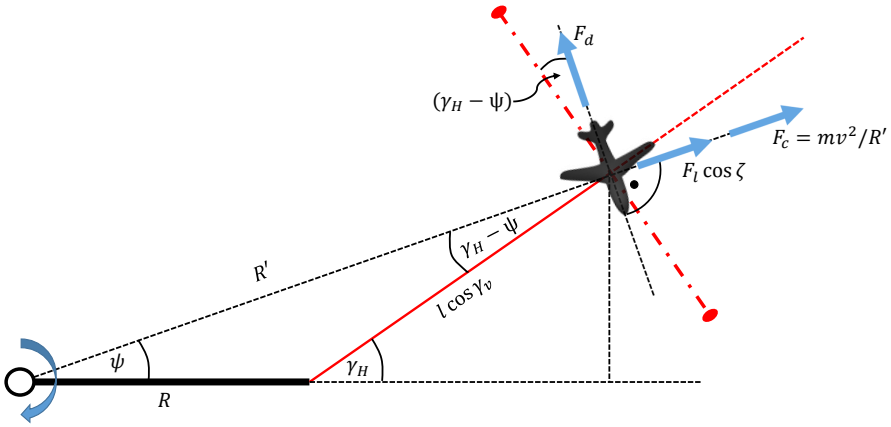

Figure 3: Drag, lift and centrifugal forces (or their components, respectively) and angles during the rotational take-off in the plane of the rotating arm. The rotating arm has a length R and the tether (in red) of l.

We consider a projection of Figure 2 onto the plane of the rotating arm, as depicted in Figure 3. Given R, ω, γ_H, γ_V and line length l, we define the angle ψ and the distance R' as:

$$\psi \doteq \arctan\left(\frac{l \cdot \cos(\gamma_V) \cdot \sin(\gamma_H)}{R + l \cdot \cos(\gamma_V) \cdot \cos(\gamma_H)}\right), \tag{15}$$

$$R' \doteq \frac{R + l\cos(\gamma_H)\cos(\gamma_V)}{\cos(\psi)}. \tag{16}$$

Then, assuming that the absolute wind speed is zero, the aircraft will develop a lift force F_l and a drag force F_d whose magnitudes are equal to

$$\begin{aligned} F_l &= \frac{1}{2}\rho A C_l (R'\omega)^2 \\ F_d &= \frac{1}{2}\rho A C_{d,eq} (R'\omega)^2 \end{aligned} \tag{17}$$

Figure 3 also shows the projections of all the considered forces (lift, drag, and centrifugal force) onto the plane of the rotating arm. The components perpendicular to the tether are the ones parallel to the dot-dashed line in the Figure.

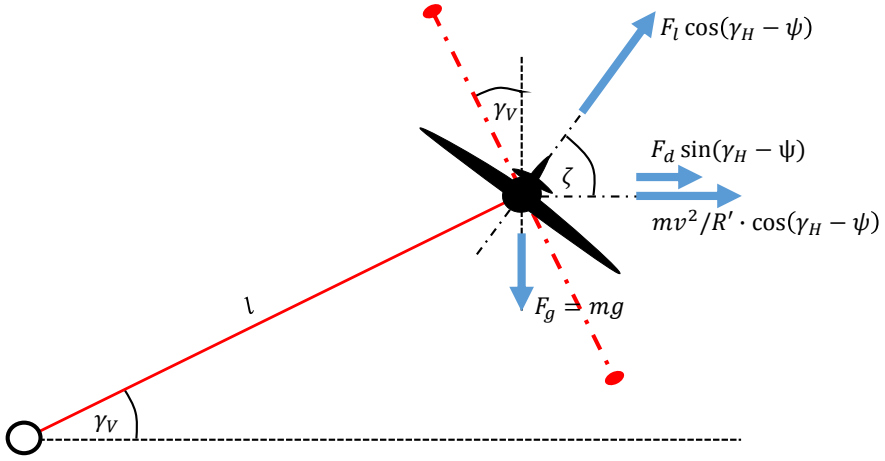

Figure 4: Drag, lift, centrifugal and gravitation forces (or their components, respectively) and angles during the rotational take-off in the plane perpendicular to the rotating arm and containing the tether.

The requirement that they cancel each other yields

$$F_d\cos(\gamma_H-\psi)=\left(F_l\cos(\zeta)+m\frac{v^2}{R'}\right)\cdot\sin(\gamma_H-\psi), \tag{18}$$

where ζ is the roll angle of the aircraft, as shown in Figure 4 which is the projection of Figure 2 onto the plane perpendicular to that of the rotating arm and containing the tether. Again, the forces perpendicular to the tether are the ones parallel to the dot-dashed line in Figure 4. Thus, the following condition must hold at the equilibrium, too:

$$\begin{aligned}F_l\cos(\gamma_H-\psi)\sin(\zeta-\gamma_V)&=mg\cdot\cos(\gamma_V)\\&+\left(m\frac{v^2}{R'}\cos(\gamma_H-\psi)+F_d\sin(\gamma_H-\psi)\right)\cdot\sin(\gamma_V).\end{aligned} \tag{19}$$

Finally, the tether tension in Eq. (13) is

$$\begin{aligned}T=&F_l\cdot\cos(\gamma_H-\psi)\cos(\zeta-\gamma_V)-mg\cdot\sin(\gamma_V)\\&+\left[F_d\sin(\gamma_H-\psi)+m\frac{v^2}{R'}\cos(\gamma_H-\psi)\right]\cdot\cos(\gamma_V)\end{aligned} \tag{20}$$

Eqs. (13)-(20) can be used to derive the power and ground area required for the rotational take-off. Since there exist many potential solutions that satisfy the equilibrium constraints (18)-(19), we choose to evaluate this take-off approach by means of numerical optimization. We compute the involved variables (i.e. ω, ζ etc.) and minimize the required mechanical power installed on the ground, $\overline{P}_{g,2}$, under certain operational constraints. More specifically, we fix the value of the arm length R and, for each pair (l,γ_V), we solve the following nonlinear program:

$$P^*_{g,2}(l,\gamma_V,R)=\min_{\zeta,\omega,\gamma_H}(RT_\perp\omega) \tag{21a}$$

$$\text{subject to} \tag{21}$$

$$\text{Eqs. (14) – (20)} \tag{21b}$$

$$\text{and } |\zeta-\gamma_V|\le\overline{\zeta} \tag{21c}$$

where the constraint (21c) is used to guarantee that the roll angle of the aircraft is such that the inner wing does not get too close to the tether, which might lead to entanglement and subsequent crash. Then, for each considered arm

length R, we compute the peak required power as

$$\overline{P}^*_{g,2}(R) = \min_{\gamma_V \in [\underline{\gamma}_V,\, \overline{\gamma}_V]} \; \max_{l \in [0,\, \bar{l}]} P^*_{g,2}(l, \gamma_V, R). \tag{22}$$

The intervals $[\underline{\gamma}_V,\, \overline{\gamma}_V]$ and $[0,\, \bar{l}]$ considered in Eq. (22) cover the range of reasonable equilibrium configurations that can occur when setting a constant vertical inclination γ_V and reeling out the line. In particular, we assume that the line is reeled-out at a constant speed $v_l \ll \omega R'$, and that a specified vertical velocity v_c of the aircraft is achieved. Then, from geometrical considerations we have that a minimum angle $\underline{\gamma}_V = \arcsin\left(\dfrac{v_c}{v_l}\right)$ shall be achieved.

The rationale behind problems (21)-(22) is the following: For a given arm length R, we fix the vertical inclination of the line during the ascend, γ_V, and we compute the required peak power over a reasonable range of line length values. Then, we search for the vertical inclination that achieves the lowest peak power. In this way, we obtain the minimal peak power, $\overline{P}^*_{g,2}(R)$, achievable with the considered arm length R and the strategy of ascending with constant vertical inclination. Finally, we repeat this procedure over a range of arm lengths $R \in [\underline{R},\, \overline{R}]$ in order to find the minimal peak power $\overline{P}_{g,2}$ required to compute our quantitative criterium **C1**:

$$\overline{P}_{g,2} = \min_{R \in [\underline{R},\, \overline{R}]} \overline{P}^*_{g,2}(R). \tag{23}$$

We resort to numerical optimization to study this approach because of its complexity, which makes it hard to derive explicit equations linking the system parameters to our quantitative criteria, as it is possible for the other take-off approaches.

Regarding the required peak onboard power $\overline{P}_{ob,2}$ and additional mass Δm, both these quantities are virtually zero in this approach. Finally, the required ground area $A_{g,2}$ is equal to πR^2_{opt}, where R_{opt} is the argument that minimizes (23).

3.3. Linear take-off with on-board propellers

In the following discussion of the linear take-off, we first analyze the on-ground acceleration phase and then the climbing phase.

3.3.1. Acceleration phase on the ground

The acceleration phase on the ground lasts until the take-off speed v^* is reached. The take-off of rigid-wing aircrafts has apparently been investigated in great detail, see e.g. [32], even though mostly for untethered aircrafts, albeit results on winch launch maneuvers also exist [16]. We briefly derive the main equations, mainly for the sake of clarity and self-consistency of the paper. The value of v^* is:

$$v^* = \sqrt{\frac{2(m + \Delta m_3)g}{\rho A C_l}}, \tag{24}$$

computed by setting $F_l = (m + \Delta m_3)\, g$ and using $F_l = \dfrac{1}{2}\rho A C_l v^{*2}$. Assuming that this speed shall be reached after a horizontal acceleration distance L, the required acceleration is $a = v^{*2}/(2L)$. The corresponding required force is then $F_{\text{g}} = (m + \Delta m_3)\, a$. The other forces acting at take-off are significantly smaller, but not negligible, namely the drag force $F_d = \dfrac{1}{2}\rho C_{d,eq} A v^{*2}$ and the viscous resistance $F_{\text{v}} = c_{\text{v}}\, v^*$, where c_{v} is the viscous friction coefficient of the system employed for the linear acceleration. Regarding the latter, here we simply employ a constant viscous friction coefficient, i.e. not depending on the vertical force applied by the aircraft on the linear motion system. One motivation for this choice is that the viscous friction has little relevance when compared to the inertia and the aerodynamic drag. Another motivation is that the additional friction force due to the weight exerted by the aircraft is also rather small, compared with the viscous friction of the electric machine and of the linear motion system without load, hence justifying the use of a constant friction coefficient. The required maximal power on the ground is

$$\overline{P}_{g,3} = v^* \left(F_{\text{g}} + F_d + F_{\text{v}}\right). \tag{25}$$

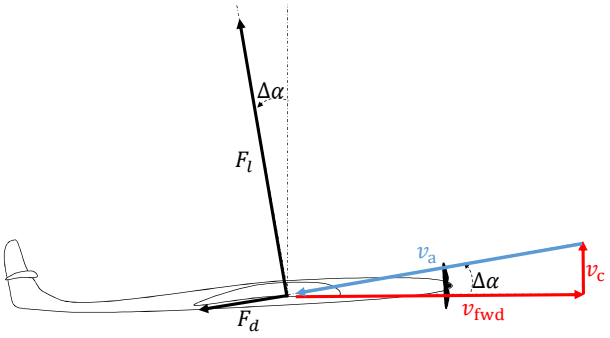

Figure 5: Schematic representation of an airplane with horizontal speed of v_{fwd} (assuming no wind) and a vertical speed of v_{c}. The lift force has a component opposite to the thrust and the drag force has a component which adds to the gravitational pull.

As regards the land occupation, we choose to fix the travel length, such that it is independent from the wing size, and we assume that the system shall be able to adapt to the widest possible range of prevalent wind conditions, i.e. the linear acceleration phase can be carried out in all directions. At the same time we assume, like we did for the vertical take-off, that the area spanned by the wings throughout the ground launching phase is considered to be occupied by the system. Thus, we obtain

$$A_{g,3} \simeq \frac{\pi L^2}{4} + \frac{\pi\lambda}{4}A. \tag{26}$$

The equations derived in this section hold both when the winch is powering the aircraft by pulling the tether and when an external linear motion system is used. In the first case, an inversion of the reeling motion has to be carried out when the aircraft starts to take-off, i.e. the winch has to revert its rotational direction from reeling-in to reeling-out. With the installed electric machine connected to the winch, dimensioned to meet the peak mechanical power experienced during the power generation phase, the available torque is rather large compared with the inertia of the winch. Thus, the motion can be inverted in very short time without compromising the take-off maneuver. When an external linear motion system is used (as we considered in section 4 and in our experimental setup [24]), there is no need to invert the reeling motion but, on the other hand, the ground station needs to be modified with additional components.

3.3.2. Powering the plane during the ascend

After the initial acceleration on the ground, the on-board propellers do not have to accelerate the plane any further, and they shall just balance the aerodynamic drag and part of the lift depending on the climbing angle. Thus, they can be rather small and consume relatively low power. In the following, we analyze the climb phase assuming the worst conditions possible, i.e. with zero prevalent wind speed, which requires the maximum on-board power.

We denote the vertical climb velocity with v_{c} again, see Figure 5. At the same time, the airplane moves horizontally with the speed v_{fwd} so that the total speed relative to the air is $v_{\text{a}} = v_{\text{fwd}} \cdot \sqrt{1 + c_{\text{r}}^2}$ with the climb ratio $c_{\text{r}} := v_{\text{c}}/v_{\text{fwd}}$. From Figure 5, it follows that $\sin(\Delta\alpha) = c_{\text{r}}/\sqrt{1 + c_{\text{r}}^2}$ and $\cos(\Delta\alpha) = 1/\sqrt{1 + c_{\text{r}}^2}$.

The vertical component of the lift force must counteract the gravitational pull and the vertical component of the drag force in order to yield a constant climb rate; i.e. the vertical equilibrium condition is $F_l \cdot \cos(\Delta\alpha) - F_d \cdot \sin(\Delta\alpha) = (m + \Delta m_3)g$. This gives

$$\frac{1}{2}\rho A C_l \sqrt{1 + c_{\text{r}}^2}\left(1 - c_{\text{r}}\frac{C_{d,eq}}{C_l}\right)v_{\text{fwd}}^2 = (m + \Delta m_3)g. \tag{27}$$

About the horizontal equilibrium, the required thrust is equal to the sum of the horizontal components of the lift and drag force, i.e.

$$\begin{aligned} F_T &= F_l \cdot \sin(\Delta\alpha) + F_d \cdot \cos(\Delta\alpha) \\ &= \frac{1}{2}\rho A C_l \sqrt{1 + c_{\text{r}}^2}\left(c_{\text{r}} + \frac{C_{d,eq}}{C_l}\right)v_{\text{fwd}}^2. \end{aligned} \tag{28}$$

Considering that the climb ratio is typically of the order of 0.1-0.2 and that the aerodynamic efficiency of the aircraft is of the order of 10-20, we assume that $C_l/C_{d,eq} \gg c_\mathrm{r}$ and obtain from Eqs. (27) and (28) the final expression for the required thrust:

$$F_T = (m + \Delta m_3)g \cdot \frac{1 + c_\mathrm{r}\frac{C_l}{C_{d,eq}}}{\frac{C_l}{C_{d,eq}} - c_\mathrm{r}} \approx (m + \Delta m_3)g \cdot \left(\frac{C_{d,eq}}{C_l} + c_\mathrm{r}\right). \tag{29}$$

The required horizontal (forward) velocity can be calculated from (27). Thus, for a desired climb rate c_r, both thrust and horizontal velocity can be computed using Eqs. (27) and (29). Similarly to what discussed for the vertical take-off, the corresponding required peak power $\overline{P}_{ob,3}$ for the propellers is then given by:

$$\overline{P}_{ob,3} = \frac{F_T}{\eta}\left(\sqrt{\frac{F_T}{2\rho A_\mathrm{prop}} + \frac{v_\mathrm{fwd}^2}{4}} + \frac{1}{2}v_\mathrm{fwd}\right). \tag{30}$$

For the propeller area A_prop, we consider two propellers (this time with horizontal axis) with a diameter of half the wing's chord and an efficiency of η.

Finally, as regards the additional on-board mass Δm_3, we consider the energy density of on-board batteries and electric motors, as in (11), and solve the resulting system of equations to obtain consistent values of $\overline{P}_{g,3}$, $\overline{P}_{ob,3}$ and Δm_3.

3.4. Winch launch

To analyze this approach, we refer to the 2-dimensional sketch of Figure 6, where the system configuration is determined by the aircraft's position (x, y). In particular, we assume that the aircraft's attitude is controlled to always have the same angle of attack, corresponding to the lift and drag coefficients C_l, C_d. We consider a quasi-stationary model (i.e. neglecting accelerations), in which the aircraft's velocity vector features a component $\dot{l}(t)$ along the tether direction, equal to the reel-in speed imposed by the winch, and a second component $v_\perp(t)$ along the direction perpendicular to the tether (see Figure 6). The absolute value of the apparent wind speed experienced by the aircraft (considering again zero external wind speed) is thus $|v_a(t)| = \sqrt{\dot{l}(t)^2 + v_\perp(t)^2}$. At each time instant t, the two velocity components are computed on the basis of the equilibrium of the lift force $F_l(t)$, drag force $F_d(t)$, tether tension $T(t)$, and gravitational force $m\,g$. The equilibrium of these forces along the direction perpendicular to the tether yields:

$$\frac{1}{2}\rho\sqrt{\dot{l}(t)^2 + v_\perp(t)^2}\left(C_l\dot{l}(t) - C_d v_\perp(t)\right) - w_l g\cos(\vartheta(t)) = 0. \tag{31}$$

Equation (31) highlights the fact that an aircraft with larger wing loading requires a larger reel-in speed for take-off, and features a lower ratio $v_\perp(t)/\dot{l}(t)$. The limiting upper bound to this ratio is the aerodynamic efficiency C_l/C_d, which is the one usually derived in the original crosswind equations where the mass is neglected (see e.g. [36]). Moreover, equation (31) has two solutions: one with very large $\dot{l}(t)$ with respect to $v_\perp(t)$, i.e. the aircraft moves roughly towards the winch, and one with very large $v_\perp(t)$ with respect to $\dot{l}(t)$, i.e. in crosswind conditions where the aircraft climbs roughly along the tangent direction to a curve with (time-varying) radius $l(t)$. The second solution is clearly the most efficient for the take-off of AWE systems. We provide more details on these aspects in section 3.5. Once the components $v_\perp(t)$, $\dot{l}(t)$ are known, we employ them to derive the speed along the (x, y) directions:

$$\begin{aligned} \dot{x}(t) &= -\dot{l}(t)\cos(\vartheta(t)) - v_\perp(t)\sin(\vartheta(t)) \\ \dot{y}(t) &= -\dot{l}(t)\sin(\vartheta(t)) + v_\perp(t)\cos(\vartheta(t)) \end{aligned} \tag{32}$$

In (32), $\dot{l}$ is considered positive when the tether is reeled in. Equations (31)-(32) form a nonlinear model of the winch launch approach, which can be integrated numerically to simulate this maneuver and evaluate the required peak power for the given parameters of the aircraft. In particular, to compute the consumed power we consider the equilibrium of forces projected on the direction of the tether (see Figure 6):

$$T(t) = \frac{1}{2}\rho A\sqrt{\dot{l}(t)^2 + v_\perp(t)^2}\left(C_l v_\perp(t) + C_d\dot{l}(t)\right) - mg\sin(\vartheta(t)). \tag{33}$$

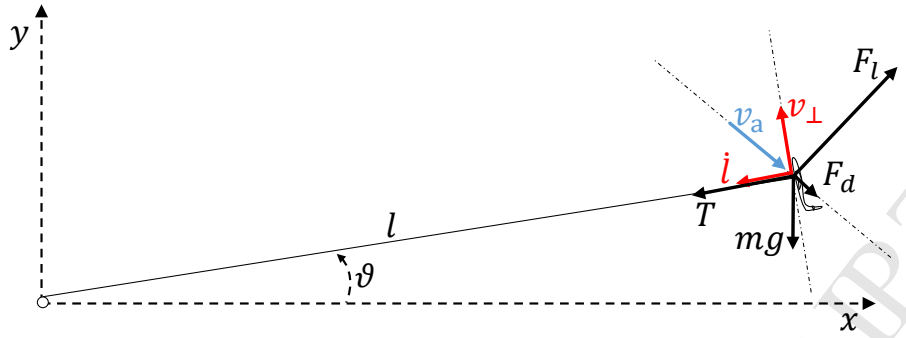

Figure 6: Schematic representation of the winch launch approach.

The mechanical power is then:

$$P_{g,4}(t) = \dot{l}(t)T(t). \tag{34}$$

The peak mechanical power $\overline{P}_{g,4}$ required by the winch launch is then computed as:

$$\overline{P}_{g,4} = \max_{t\in[0,t^*]} P_{g,4}(t), \tag{35}$$

where $t = 0$ is the starting instant of the maneuver, and t^* is the instant when the target height h is reached. Finally, regarding the required ground area, we denote with $\underline{l}(h)$ the minimum initial tether length such that the target altitude h can be reached with zero external wind. In order to adapt to all possible wind directions, the corresponding required ground area is then equal to:

$$A_{g,4} = \pi \underline{l}(h)^2. \tag{36}$$

The value of $\underline{l}(h)$ can be computed numerically by simulating the model (31)-(32) with different initial values of tether length $l(0)$, starting from a relatively large one and decreasing it until the target h cannot be reached anymore. We note that equation (36) might give conservative results, for the following considerations. (a) First, trading off some launching efficiency, the aircraft does not necessarily need to align with the wind to launch: lateral wind is acceptable up to a certain degree, such that a cross-shaped pattern, corresponding to two orthogonal runways, could be enough. (b) Second, the ground area strictly occupied by the glider is an annulus, and not the whole circle of $\underline{l}(h)$. In this sense equation (36) could be adapted to be an annulus of the form $\pi\,(\underline{l}(h) - l^\star)^2$, where $l^\star$ is related to the take-off distance, the need to maneuver the aircraft and prepare it for take-off, and possibly some minimal altitude margin. On the other hand, it is difficult to say whether the land in the inner part of the annulus could be used for other purposes or not, even with a take-off platform some meters above ground, due to the tether catenary and the risk of entangling with objects before or during the take-off. In both (a) and (b), the resulting area would be a fraction of $A_{g,4}$ but still depend quadratically on the minimal initial tether length. For completeness, in section 3.5 we also comment on the results obtained by considering an annulus instead of equation (36).

3.5. Results and Discussion

In this section, we apply the results presented so far to evaluate the criteria **C1**-**C3**. In particular, we consider three different wing sizes and corresponding design parameters as shown in Tables 1-2. The design parameters are chosen according to typical values encountered in the field of AWE [1]. The obtained results are used, together with the qualitative criteria **C4**-**C5**, to discuss the considered take-off approaches and draw conclusions on their viability. For the computation of **C1**, the mechanical power P_m^* is calculated with Eq. (3) with a wind speed $W = 15$ m/s. Regarding the energy density of on-board batteries and the power density of on-board motors, we considered $E_{\text{batt}} = 720$ kJ/kg and $E_{\text{mot}} = 2.5$ kg/kW [7]. The viscous friction coefficient c_v for the linear take-off has been estimated based on known values from electric machines and linear motion systems, with sizes comparable to the ones considered in this study. Table 2 shows in bold the results obtained according to the analysis described in sections 3.1-3.4, including the

Table 1: Design parameters considered for the assessment of the different take-off concepts. The parameters given here are common to two or more take-off approaches.

Parameter	**Aircraft 1**	**Aircraft 2**	**Aircraft 3**
Wing span d (m)	5	10	20
Aspect ratio λ		10	
Chord d/λ (m)	0.5	1	2
Wing area A (m^2)	2.5	10	40
Wing loading $w_l = m/A$ (kg/m^2)		15	
Aircraft mass m (kg)	37.5	150	600
Lift coefficient C_l		1	
Drag coefficient $C_{d,eq}$		0.1	
Desired vertical velocity v_c (m/s)		1	
Propeller efficiency η		0.7	
Target height h (m)		100	
Energy density of on-board batteries E_{batt} (kJ/kg)		720	
Power density of on-board motors E_{mot} (kW/kg)		2.5	
Peak mechanical power P_m^* with $W = 15$ m/s (kW)	75	300	1200

values of $\overline{P}_{g,i}$, $\overline{P}_{ob,i}$, Δm_i, and $A_{g,i}$. Finally, Table 3 summarizes the values of the scaling factors that define the criteria **C1**-**C3**, obtained with the parameters of Tables 1-2. Before drawing a final assessment, we briefly comment on the results obtained with each approach.

Vertical take-off. As expected, this approach requires the largest amount of additional on-board power (about 20% of the peak mechanical power of the system) and of additional mass (20% of the aircraft mass), see Table 3. On the other hand, the required ground area turns out to be the smallest among the three approaches. The additional complexity (criterium **C4**) can be substantial, since the aircraft and on-board equipment have to be designed to sustain the large accelerations experienced during crosswind flight, and since large electric on-board power is required. This might require a completely new design of the wing. The additional mass also leads to a larger cut-in speed for the generator, since a larger wind speed will be required for the system to be able to remain airborne during power generation. Moreover, in a deeper analysis the presence of the propellers will have a detrimental influence on the aerodynamics, hence either requiring a larger wing for the same power, or giving lower power for the same size. These aspects lead in turn to a reduced capacity factor. The possibility to take-off in a large range of wind conditions (criterium **C5**) is in principle given, although more detailed studies should be carried out to assess whether the control surfaces and the propellers can effectively stabilize the aircraft during the ascend with relatively strong wind.

Rotational take-off. While the results for the vertical and linear approaches are derived in a straightforward way from the equations presented in sections 3.1 and 3.3, some more comments are due on the results pertaining to the rotational take-off. The application of the optimization procedure described in section 3.2 provides several interesting outcomes. First, it turns out that there exist a minimal arm length $\underline{R}$ that allows the system to achieve vertical inclination angles larger than the minimum required one, i.e. $\underline{\gamma}_V$. The value of $\underline{R}$ mainly depends on the wing loading w_l, while it is not affected significantly by the wing size. This is shown in Figure 7 which presents the curves of maximum γ_V values that can be achieved as a function of line length l, for various combinations of wing loading w_l, arm length R and wingspan d.

The main explanation for this phenomenon is that the aerodynamic forces have to counteract the centrifugal force (see section 3.2), which decreases as the arm length R increases. For the wing loading and minimal vertical inclination values chosen for our comparison, i.e. $w_l = 15\,\text{kg/m}^2$ and $\gamma_V = 40°$, we obtain $\underline{R} \simeq 30\,\text{m}$, as reported in Table 2.

Secondly, the required peak power increases with γ_V, since the equilibrium conditions (18)-(19) become less favorable and a larger rotational speed is required to generate enough lift to maintain the desired vertical inclination. This is shown in Figure 8. Hence, for the sake of minimizing the required additional power, the minimum vertical inclination is chosen.

Lastly, the peak mechanical power decreases with the arm length and approaches an asymptotic value, see Figure 9. The reason is that, as the centrifugal force decreases (i.e. R increases), the aerodynamic forces only have to balance

Table 2: Parameters considered for the assessment of the different take-off concepts. The parameters given here are specific to each take-off approach. Bold-faced parameters are the results obtained according to the assumptions and analysis described in sections 3.1-3.4.

Parameter	**Aircraft 1**	**Aircraft 2**	**Aircraft 3**
Vertical take-off			
Propeller diameter d/λ (m)	0.5	1	2
Peak additional on-board power $\overline{P}_{ob,1}$ (kW)	**14**	**56**	**223**
Additional on-board mass Δm_1 (kg)	**8**	**30**	**120**
Required ground area $A_{g,1}$ (m^2)	**20**	**80**	**315**
Rotational take-off			
Maximum angle between the wings and the plane perpendicular to the line $\overline{\zeta}$ (deg)	50		
Reel-out speed of the line v_l (m/s)	1.6		
Minimum vertical inclination $\underline{\gamma}_V$ (deg)	**40**		
Maximum vertical inclination $\overline{\gamma}_V$ (deg)	90		
Minimum arm length $\underline{R}$ (m)	**30**		
Maximum arm length $\overline{R}$ (m)	50		
Optimal arm length R_{opt} (m)	**50**		
Maximal angular velocity ω (rad/s)	**0.4**		
Maximal tangential velocity of the tip of the arm ωR (m/s)	**20**		
Peak additional ground power $\overline{P}_{g,2}$ (kW)	**3**	**12**	**47**
Additional on-board mass Δm_2 (kg)	0		
Required ground area $A_{g,2}$ (m^2)	**7854**		
Linear take-off with on-board propellers			
Ground travel distance L (m)	12		
Viscous friction coefficient c_v (kg/s)	0.1	0.3	1
Take-off speed v^* (m/s)	**15.7**		
Propeller's diameter $d/(2\lambda)$ (m)	0.25	0.5	1
Peak additional ground power $\overline{P}_{g,3}$ (kW)	**8**	**31**	**124**
Peak additional on-board power $\overline{P}_{ob,3}$ (kW)	**2**	**9**	**37**
Additional on-board mass Δm_3 (kg)	**2**	**5**	**20**
Required ground area $A_{g,3}$ (m^2)	**132**	**192**	**428**
Winch launch			
Peak additional ground power $\overline{P}_{g,4}$ (kW)	0		
Peak additional on-board power $\overline{P}_{ob,4}$ (kW)	0		
Additional on-board mass Δm_4 (kg)	0		
Required initial tether length $\underline{l}$ (m)	**130**		
Required ground area $A_{g,4}$ (m^2)	**53100**		

Table 3: Results for the quantitative performance criteria **C1**, **C2**, and **C3** (Eqs.(5)-(7)) with the parameters of Table 1.

	C1: power		**C2**: mass	**C3**: area	
Concept	$\eta_{P_g,i}$ (%)	$\eta_{P_{ob},i}$ (%)	$\eta_{m,i}$ (%)	$\underline{A}_{g,i}$	$\eta_{A_g,i}$ (%)
Vertical	0	19	21	0	$\frac{\pi\lambda}{4}$
Rotational	4	0	0	$\frac{\pi R^2}{4}$	0
Linear	11	3	5	$\frac{\pi L^2}{4}$	$\frac{\pi\lambda}{4}$
Winch launch	0	0	0	$\pi\underline{l}(h)^2$	0

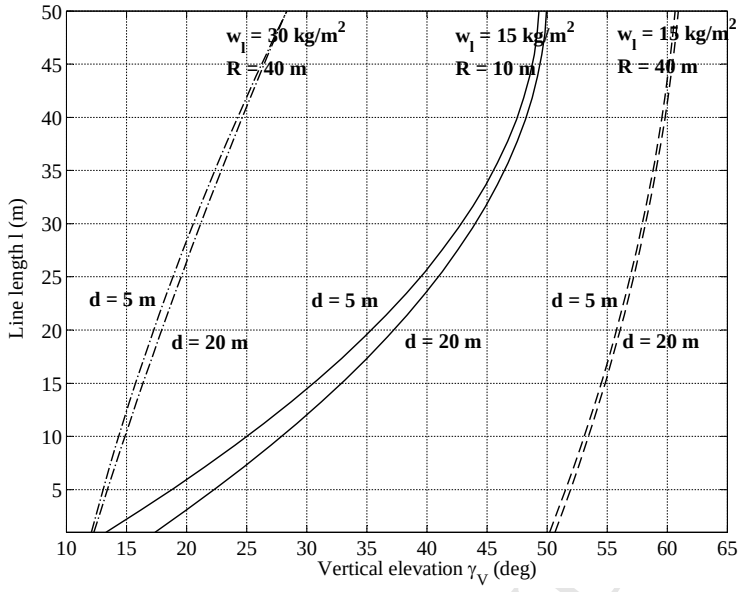

Figure 7: Analysis of the rotational take-off. Curves showing the maximum elevation angle γ_V that can be achieved as a function of the line length with $w_l = 15\,\mathrm{kg/m^2}$ and $R = 10\,\mathrm{m}$ (solid lines), $w_l = 15\,\mathrm{kg/m^2}$ and $R = 40\,\mathrm{m}$ (dashed), and $w_l = 30\,\mathrm{kg/m^2}$ and $R = 40\,\mathrm{m}$ (dash-dotted). For each combination of w_l and R, two values of wingspan ($d = 5\,\mathrm{m}$ and $d = 20\,\mathrm{m}$) are shown.

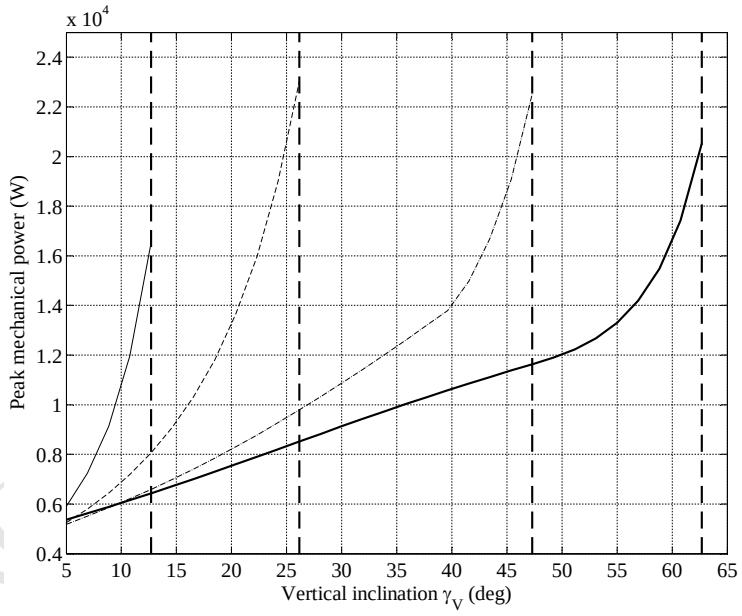

Figure 8: Analysis of the rotational take-off. Curves showing the peak ground mechanical power $P^*_{g,2}$ for $l = 1\,\mathrm{m}$ as a function of the elevation angle γ_V and with $R = 10\,\mathrm{m}$ (thin solid line), $R = 20\,\mathrm{m}$ (dashed), $R = 40\,\mathrm{m}$ (dash-dotted) and $R = 80\,\mathrm{m}$ (thick solid line). The vertical dashed lines indicate the maximum elevation angle achievable for each considered arm length. Wing span $d = 10\,\mathrm{m}$, wing loading $w_l = 15\,\mathrm{kg/m^2}$.

365 the weight of the aircraft. This condition leads asymptotically, for growing R, to a minimally required tangential speed

and corresponding forces which then determine the required power to rotate the arm. In order to restrict our analysis to a finite value of R, we choose an upper bound of $\overline{R} = 50$ m, which is then the optimal value according to Eq. (23).

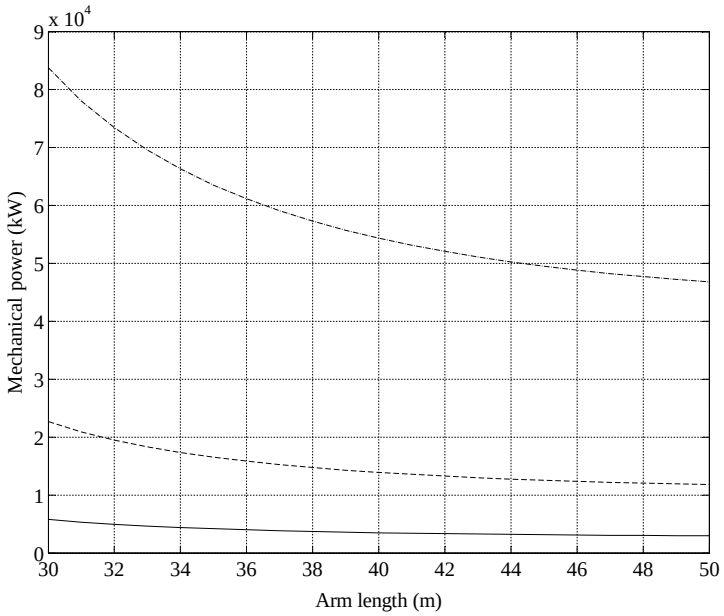

Figure 9: Analysis of the rotational take-off. Curves showing the peak ground mechanical power $P^*_{g,2}$ for $l = 1$ m as a function of the arm length R for $d = 5$ m (solid), $d = 10$ m (dashed), and $d = 20$ m (dash-dotted). Wing loading $w_l = 15$ kg/m^2.

Due to the mentioned findings, the rotational start-up results in a rather low value of additional power required on ground and in zero on-board power, as well as zero additional mass, but a very large ground-area occupation as compared with the other two approaches, see Tables 1-3. Such a land occupation is fundamentally linked to the wing loading as discussed above. Hence, it is not possible to decrease the land occupation below a minimum threshold by increasing the installed power or decreasing the wing size. As a matter of fact, the minimum ground occupation is quite large for a reasonable wing loading.

As regards complexity (**C4**), this is expected to be large, considering that the system would feature a 50-m-long rigid arm whose tip rotates with a tangential speed of about 20 m/s. Moreover, the main winch should rotate as well with many full revolutions while at the same time reeling the line, which poses a challenge for the winch mechanics and the electrical connections. The manufacturing and installation costs of such a structure could be comparable to those of a traditional wind turbine and appear to be prohibitive for the economic viability of the approach. Finally, about wind adaptation (**C5**) it is unclear how this concept would handle a strong prevalent wind during take-off, when the relative wind speed could change by e.g. ±10 m/s during a half turn, with the aircraft speed relative to ground of about 20 m/s.

Linear take-off. The required peak power installed on the ground for this approach is larger than that of the rotational take-off, however with a significantly smaller required area. Moreover, differently from the rotational take-off, in the linear take-off the ground area and required power can be easily traded off. As regards the on-board power and additional mass, they result to be about six times smaller than for the vertical take-off. The required ground occupation is comparable to the vertical take-off and dominated by the wing size when scaling up, hence it turns out to be favorable. About the complexity of the approach, this appears to be small, since in principle one could envision a solution where the winch used to generate power is also employed in the initial phase of the take-off, e.g. by means of a clutch to (dis-) engage a linear motion system to accelerate the aircraft. Similarly, the on-board propellers and batteries are necessary in any case to power the on-board control systems. Hence, the use of slightly larger and more powerful on-board motors does not appear to be critical. Moreover, the on-board propellers can also be used to re-

charge the batteries to supply energy to the control system during long periods of power generation. Finally, since the whole setup can be turned, the take-off is independent of the current prevalent wind direction.

Winch launch. This approach requires zero additional power, both on-ground and on-board, and consequently zero additional mass. In fact, it turns out that, independently of the aircraft's size, with the considered parameters the peak required power for take-off is about 47% of the peak mechanical power. This is shown in Figure 10, where the required power during the ascend, normalized by the corresponding peak mechanical power, is presented. Since the winch is installed on the GU and sized to provide the peak mechanical power, no additional power is needed. The instant that requires most power is the initial one, as intuition suggests.

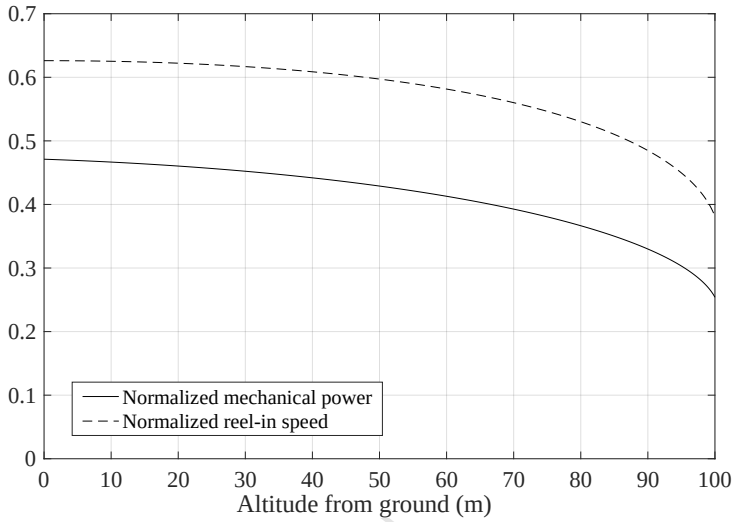

Figure 10: Analysis of the winch launch. Curves show the normalized power (solid) and reel-in speed (dashed) as a function of the altitude above ground, up to the target height $h = 100\,\mathrm{m}$.

Figure 10 also shows the required reel-in speed, normalized by the take-off speed of the aircraft of 15.7 m/s (computed using (24) with no additional on-board mass). The maximum reel-in speed is also experienced at the first instant of the take-off, and it amounts to about 62% of the take-off speed for the considered parameters, i.e. about 9.8 m/s. Clearly, both the peak power and reel-in speed increase with the wing loading: as an example, with $w_l = 25\,\mathrm{kg/m^2}$ and the same aerodynamic coefficients the required power increases to 101% of the peak power, and the initial reel-in speed to 12.6 m/s. The launching trajectory in (x, y) coordinates for the considered parameters is depicted in Figure 11. This trajectory is independent of the wing's size and also of the wing loading, since with larger wing loading the same pattern is followed, but with higher speed than with lower wing loading. Finally, Figure 11 also shows a second possible path, obtained by solving equations (31)-(32) for the second feasible equilibrium, i.e. with much larger $\dot{l}$ value than $v_\perp$: as anticipated in section 3.4, such a solution corresponds to keeping the aircraft on a trajectory roughly parallel to the ground, and does not lead to an effective take-off.

Following the considerations made in section 3.4, we computed the required ground area also considering an annulus of area $\pi\,(\underline{l}(h)^2 - l^{\star 2})$ instead of the whole circle of radius $\underline{l}(h)$, where we considered $l^\star = 10\,\mathrm{m}$ (a reasonable minimal value to properly maneuver the aircraft and prepare for the launch). The resulting area is about 7800 m^2, similar to that of the carousel launch and about seven times smaller than considering the full circle (see Table 3), but still about 20 times larger than the linear and vertical launch approaches.

Discussion. The results presented so far indicate that both the vertical and the rotational take-off require extensive modifications of the AWE system, which will have a strong influence on the design and require significant additional equipment. On the contrary, the winch launch does not require any modifications to the glider, but requires a very large land area, as initially speculated. On the other hand, the linear take-off approach will have relatively low impact on the system design. If the main winch can also be used for the acceleration phase, the additional equipment required

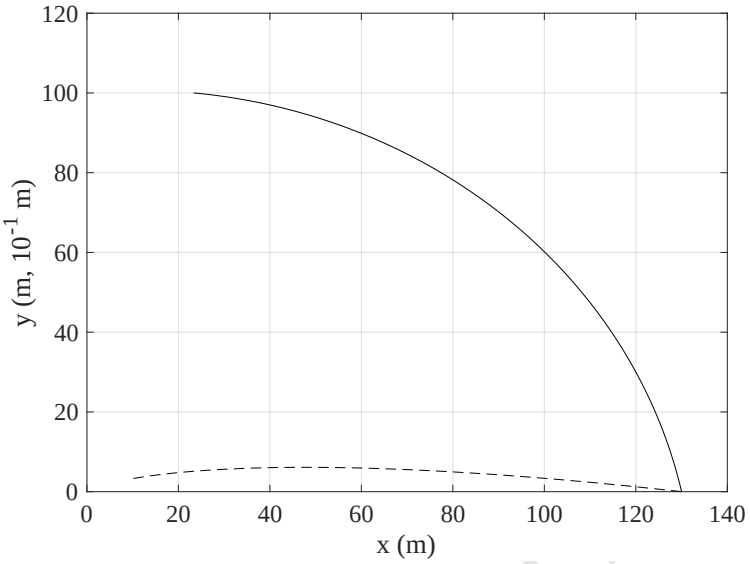

Figure 11: Analysis of the winch launch. Curves show the (x, y) trajectory obtained with a feasible solution where $\dot{l} \ll v_\perp$ (solid line, both x and y values in m), and one where $\dot{l} \gg v_\perp$ (dashed line, x in m, y values in 10^{-1} m for the sake of visualization).

is in fact reduced to a minimum. Such a solution could be achieved by installing a clutch to engage/disengage the linear motion system from the winch and using the latter to accelerate the aircraft. Another approach could be to carry out a short winch launch, in which the reeling direction is quickly reverted from reel-in to reel-out. In terms of mechanical power, the linear take-off provides a good tradeoff between on-board and on-ground power. Moreover, the additional on-board components like batteries and small propellers will have further applications, like powering the on-board electronics. Finally, the land occupation of the linear take-off is almost as small as that of the vertical one. For these reasons, we decide to focus on the linear take-off for rigid-wing AWE systems with ground-based electric generation. This approach will be analyzed in more detail in the following section.

4. Simulation of a linear take-off approach

In this section, we further study, by means of numerical simulations, the linear take-off combining ground motors and on-board propellers. We first introduce a dynamical model of the system, then we describe the control algorithms to carry out the take-off maneuver, finally we present the simulation results and compare them with the static equations derived in section 3.3.

4.1. A dynamical model for linear take-off

We consider a GU composed of a winch, where the aircraft's tether is coiled, and of a linear motion system, whose aim is to accelerate the aircraft up to take-off speed, see Figure 12. The winch rotation is controlled by a geared motor/generator M_1, which is the main electrical machine of the AWE system, responsible for converting mechanical power into electricity during the power generation cycles. The linear motion system consists of a slide, carrying the aircraft during take-off, that can move along rails. The slide motion is controlled by a second geared motor M_2 through a transmission system (e.g. a belt). The slide is equipped with sheaves that guide the tether from the winch to the attachment point on the aircraft. This system can be described by a hybrid dynamical model: a first operating mode (Figure 12(a)) describes the system's behavior from zero speed up to the take-off, when the aircraft and the slide can be considered as a unique rigid body; a second operating mode (Figure 12(b)) describes the aircraft motion after take-off, when it is separated from the slide. For the sake of simplicity, we consider a two-dimensional motion only in the second mode, i.e. vertical and horizontal displacements and pitch rotation of the aircraft, assuming that suitable

stabilizing systems act on the on-board actuators (rudder and ailerons) in order to keep the roll and yaw angles at small values, counteracting potential lateral wind turbulence. Moreover, we assume that no wind opposite to the take-off direction is present, i.e. the take-off is carried out only by means of the ground motors and on-board propellers. In case of substantial wind, we assume the system to be capable to orient the rails according to the wind direction to take advantage of the additional apparent wind velocity, hence reducing the take-off speed. Thus, the conditions simulated here provide the worst-case in terms of required power, in line with the analysis of section 3.3. All the equations presented in the following have been derived by applying Newton's second law of motion.

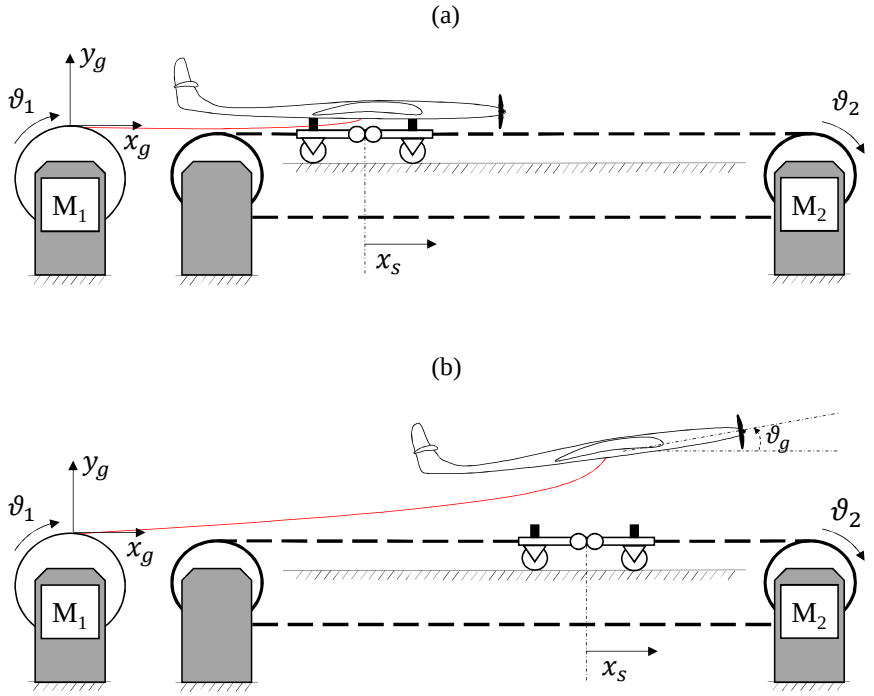

Figure 12: Sketch of the system considered to simulate the linear take-off procedure. (a) First operating mode, with the aircraft carried by the slide up to take-off speed; (b) second operating mode, with the aircraft gaining altitude by means of the on-board propeller.

The state of the model, i.e. the variables that describe completely and univocally its configuration at any time instant t, is given by $x(t) \doteq [\vartheta_{M_1}(t),\ \dot{\vartheta}_{M_1}(t),\ \vartheta_{M_2}(t),\ \dot{\vartheta}_{M_2}(t),\ x_g(t),\ \dot{x}_g(t),\ y_g(t),\ \dot{y}_g(t),\ \vartheta_g(t),\ \dot{\vartheta}_g(t)]^T$, where ϑ_{M_1} is the angular position of the winch, $\dot{\vartheta}_{M_1} \doteq \frac{d\vartheta_{M_1}}{dt}$ its angular speed, ϑ_{M_2}, $\dot{\vartheta}_{M_2}$ are the angular position and speed of the motor that controls the linear motion system, $x_g(t)$, $\dot{x}_g(t)$, $y_g(t)$, $\dot{y}_g(t)$, the horizontal (x) and vertical (y) positions and speeds of the aircraft's center of gravity in an inertial reference frame. The latter has its center at the point where the tether exits the winch, the x_g-axis parallel to the ground and the y_g-axis vertical and pointing upwards (see Figure 12). Finally, $\vartheta_g(t)$, $\dot{\vartheta}_g(t)$ are the aircraft's pitch angle and its rate. The manipulated inputs available to control and operate the system are denoted with $u(t) \doteq [C_{M_1}(t),\ C_{M_2}(t),\ F_T(t)]^T$ where C_{M_1}, C_{M_2} are the torques applied by the two electrical machines, and F_T is the thrust force exerted by the on-board propeller. The motor torques considered in the model are taken after any gear that can be installed between the motor and the winch (respectively the belt's pulley) to adapt the motor's torque/speed profile to the application. In the following, for the sake of simplicity we denote with x_j (resp. u_j) the j^{th} component of the state (resp. input) vector defined above. Assuming that the linear motion system is realized by a belt, driven by a pulley directly attached to the shaft of motor M_2, and neglecting its

elasticity, the model in the first operating mode is given by the following equations:

$$\begin{aligned}
\dot{x}_1(t) &= x_2(t) \\
\dot{x}_2(t) &= \frac{1}{J_{M_1}}(r_{M_1}\, T(t) - \beta_{M_1}\, x_2(t) + u_1(t)) \\
\dot{x}_3(t) &= x_4(t) \\
\dot{x}_4(t) &= \frac{1}{J_{M_2} + (m_s + m)\, r_{M_2}^2}\,(r_{M_2}\,(-T(t) + \\
&\quad -F_d(t)\,\cos(\Delta\alpha(t)) + \\
&\quad +F_l(t)\,\sin(\Delta\alpha(t)) - \beta_s\, r_{M_2}\, x_4(t)) \\
&\quad -\beta_{M_2}\, x_4(t) + u_2(t)) \\
\dot{x}_5(t) &= x_6(t) \\
\dot{x}_6(t) &= r_{M_2}\, \dot{x}_4(t) \\
\dot{x}_7(t) &= x_8(t) \\
\dot{x}_8(t) &= 0 \\
\dot{x}_9(t) &= x_{10}(t) \\
\dot{x}_{10}(t) &= 0.
\end{aligned} \tag{37}$$

In (37), r_{M_1} is the radius of the winch (assuming for simplicity that the latter is directly connected to the motor/generator), r_{M_2} the radius of the pulley that links motor M_2 to the belt, J_{M_1}, J_{M_2} the moments of inertia of the winch and of the pulley plus their respective motors, β_{M_1}, β_{M_2} their viscous friction coefficients, m_s the mass of the slide, β_s the viscous friction coefficient of the belt/slide/rail system, m the mass of the aircraft. Similarly to section 4.3, we employ a constant friction coefficient in the simulation study, estimated on the basis of available data-sheets and knowledge of linear motion systems with size comparable to the one considered here. The angle $\Delta\alpha$ is defined as:

$$\Delta\alpha(t) = \arctan\left(\frac{-\dot{y}_g}{\dot{x}_g}\right), \tag{38}$$

i.e. the angle between the velocity vector of the aircraft and the inertial x_g-axis, measured positive if the y_g-axis component of the velocity is negative, i.e. if the aircraft is descending. T is the tension force on the tether:

$$T(t) = \min\left(0, k_t\,\left(\|(x_g(t), y_g(t))\|_2 - r_{M_1}\, x_1(t)\right)\right), \tag{39}$$

where k_t is the stiffness of the tether, assumed constant for simplicity. The saturation to 0 in Eq. (39) accounts for the fact that the tether can only transfer force when under tension, i.e. when its length $r_{M_1}\, x_1(t)$ is smaller than the position of the aircraft relative to its attachment point on the ground. Finally, F_l and F_d are, respectively, the aerodynamic lift and drag forces developed by the aircraft, computed as:

$$\begin{aligned}
F_l(t) &= \tfrac{1}{2}\rho A C_l(\alpha(t)) \cdot \|(\dot{x}_g(t), \dot{y}_g(t))\|_2^2 \\
F_d(t) &= \tfrac{1}{2}\rho A C_{d,eq}(\alpha(t)) \cdot \|(\dot{x}_g(t), \dot{y}_g(t))\|_2^2
\end{aligned} \tag{40}$$

where $\alpha(t)$ is the angle of attack:

$$\alpha(t) = \vartheta_0 + \Delta\alpha(t) + x_9(t). \tag{41}$$

The angle ϑ_0 is a fixed setting for the wings' orientation, such that if the aircraft is flying horizontally (i.e. $\Delta\alpha = 0$) at zero pitch angle then we have $\alpha = \vartheta_0$. The considered courses of C_l, C_d as a function of α are shown in Figure 13 and correspond to a finite wing with Clark-Y profile [40]. The same figure also shows the chosen trimming for ϑ_0. In this simulation study, we neglect additional effects like the change of drag with the wingspan and non-steady-state effects, since these aspects pertain to further levels of approximation and detail. This is beyond the scope of this simulation study, which is meant to capture possible differences, with respect to the analysis of section 3.3, due to the inertia/friction of the winch and the control performance with limited inputs. The addition of more sophisticated aerodynamic models will not alter the overall picture significantly because most of the power during the take-off is required to overcome the inertia of the system.

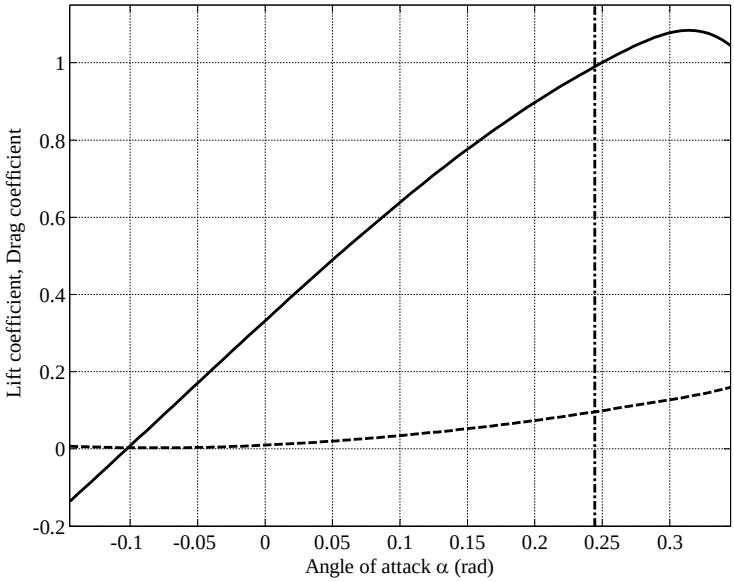

Figure 13: Lift (solid line) and drag (dashed) coefficients used in the dynamical simulation model of the take-off phase, and initial wing trimming ϑ_0 (dash-dotted line).

We denote the initial state with x_0^I, which is required to simulate the model (37), i.e. $x(0) = x_0^I$. In particular, we choose the initial condition

$$x_0^I = \left[\frac{l_0}{r_{M_1}},\, 0,\, 0,\, 0,\, x_{g,0},\, 0,\, 0,\, 0,\, 0,\, 0\right]^T, \tag{42}$$

meaning that the motors, the slide and the aircraft are initially at rest, a length l_0 of tether is reeled out and the distance of the aircraft's starting position from the attachment point of the line on the winch is equal to $x_{g,0}$, with $x_{g,0} > l_0$ so that the tether is not exerting any force on the glider and the slide (see Eq. (39)).

The switch between the first and the second operating mode takes place at the time instant t^* defined as:

$$t^* = \min\left(\tau \geq 0 \,:\, F_l(\tau)\cos(\Delta\alpha(\tau)) > mg\right). \tag{43}$$

Thus, t^* represents the time instant when the vertical lift force developed by the glider is larger than its weight, hence obtaining a positive vertical acceleration. The initial condition x_0^{II} of the model that describes the system in the second operating mode is then given by:

$$x_0^{II} = x(t^*), \tag{44}$$

i.e. the state of the system in the first operating mode at the switching instant t^*. The model equations for the second

operating mode are the following:

$$\begin{aligned}
\dot{x}_1(t) &= x_2(t) \\
\dot{x}_2(t) &= \frac{1}{J_{M_1}}(r_{M_1}\, T(t) - \beta_{M_1}\, x_2(t) + u_1(t)) \\
\dot{x}_3(t) &= x_4(t) \\
\dot{x}_4(t) &= \frac{1}{J_{M_2} + m_s\, r_{M_2}^2}\,(-r_{M_2}^2\, \beta_s\, x_4(t) - \beta_{M_2}\, x_4(t) \\
&\quad + u_2(t)) \\
\dot{x}_5(t) &= x_6(t) \\
\dot{x}_6(t) &= \frac{1}{m + m_t(t)}\,(F_l(t)\, \sin(\Delta\alpha(t)) \\
&\quad - F_d(t)\, \cos(\Delta\alpha(t)) + \cos(x_9(t))\, u_3(t)) \\
\dot{x}_7(t) &= x_8(t) \\
\dot{x}_8(t) &= \frac{1}{m + m_t(t)}\,(F_l(t)\, \cos(\Delta\alpha(t)) \\
&\quad + F_d(t)\, \sin(\Delta\alpha(t)) \\
&\quad - (m + m_t(t))\, g + \sin(x_9(t))\, u_3(t)) \\
\dot{x}_9(t) &= x_{10}(t) \\
\dot{x}_{10}(t) &= \omega_\beta(-\Delta\alpha(t) - x_{10}(t)),
\end{aligned} \tag{45}$$

where m_t is the mass of the tether that has been reeled out:

$$m_t(t) = \rho_t\, \pi\, r_t^2\, r_{M_1}\, x_1(t) \tag{46}$$

with ρ_t and r_t being respectively the density and the radius of the tether. Regarding the last two equations in Eq. (45), which describe the behavior of the pitch angle, we assume for simplicity that an active control system actuates the elevator in order to track the angle $\vartheta_{g,ref} \doteq -\Delta\alpha(t)$ with no offset, and that the resulting closed-loop dynamical behavior is given by a first-order system with time constant $\frac{1}{\omega_\beta}$, where ω_β is a constant parameter. In this way, if a steady state is attained during the ascend, the corresponding angle of attack will match the parameter ϑ_0, see Eq. (41). Note that the pitch angle ϑ_g (i.e. x_9) affects how the thrust force u_3 exerted by the propeller acts on the horizontal and vertical dynamics of the aircraft, hence providing a further coupling between the pitch dynamics and the aircraft translational motion.

Eqs. (37)-(46) provide the hybrid model that we use to refine the results given in section 3. However, this model cannot be simulated without first implementing suitable feedback controllers, since the open-loop behavior of the system is not stable. In the next section, we briefly describe the controllers we employ to carry out the numerical simulations.

4.2. Control design

A block-diagram of the employed control approach is shown in Figure 14. The control objectives are different between the first and second operating mode. In the first mode, the winch motor M_1 has to accelerate fast enough, such that the tether tension is always zero, but avoiding at the same time that an excessive tether length is reeled-out, to limit the line sag. At the same time, the slide motor M_2 has to accelerate from zero to take-off speed. To achieve these goals, we employ the following proportional controllers:

$$\begin{aligned}
u_1(t) &= K_{M_1}(\dot{x}_{g,to} - r_{M_1}\, x_2(t)) \\
u_2(t) &= K_{M_2}(\dot{x}_{g,to} - r_{M_2}\, x_4(t))
\end{aligned} \tag{47}$$

where K_{M_1}, K_{M_2} are the controllers' gains, and $\dot{x}_{g,to}$ is a reference speed.

In the second operating mode, the winch motor M_1 shall maintain a reel-out speed that matches that of the aircraft, again to keep the tether tension at a low value. The motor M_2 shall brake and stop the slide. Finally, the on-board propeller shall track a desired vertical velocity $x_{8,ref} = \dot{y}_{g,to}$. To obtain these goals, we employ the following proportional controllers for the motors:

$$\begin{aligned}
u_1(t) &= K_{M_1}(\|(x_6(t), x_8(t))\|_2 - r_{M_1}\, x_2(t)) \\
u_2(t) &= -K_{M_2} r_{M_2}\, x_2(t),
\end{aligned} \tag{48}$$

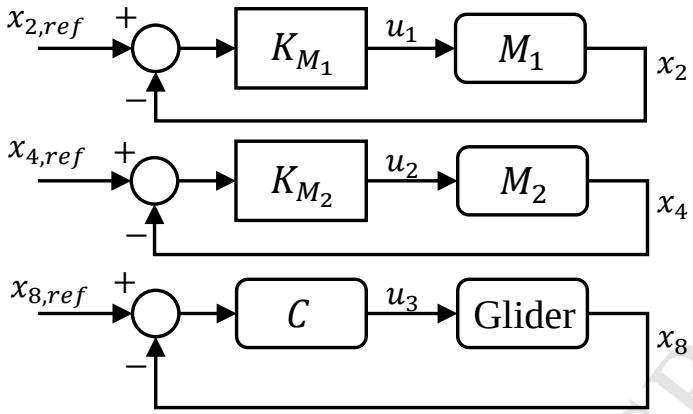

Figure 14: Block-diagram of the control approach employed for the simulations. The reference speed values for the winch and slide motors are $x_{2,ref} = x_{4,ref} = \dot{x}_{g,to}$ in the first operating mode, and $x_{2,ref}(t) = \|(x_6(t), x_8(t))\|_2$, $x_{4,ref} = 0$ for the second operating mode, while the reference vertical speed for the glider is $x_{8,ref} = \dot{y}_{g,to}$, see also equations (47)-(49). The motors, glider and glider's controller C are dynamical systems, while the gains K_{M_1}, K_{M_2} are static.

while for the propeller we implement a dynamical cascade controller whose transfer function in the Laplace domain is the following

$$C(s) \doteq \frac{U_3(s)}{E_{\dot{y}_g}(s)} = K_T \frac{\left(1 + \frac{s}{w_{z,1}}\right)\left(1 + \frac{s}{w_{z,2}}\right)}{s\left(1 + \frac{s}{w_p}\right)} \tag{49}$$

where s is the Laplace variable, $U_3(s)$ and $E_{\dot{y}_g}(s)$ are the Laplace transforms of the propeller thrust signal $u_3(t)$ and of the tracking error $e_{\dot{y}_g}(t) \doteq \dot{y}_{g,to} - \dot{y}_g(t)$, respectively, and K_T, $w_{z,1}$, $w_{z,2}$ and w_p are design parameters. The need for a slightly more complex controller (49) for the propeller, with respect to the simple proportional gains (47)-(48) used for the motors, stems from the presence of additional dynamics in the glider, for example due to the interaction between the pitch dynamics and the translational motion, that need to be compensated in order to avoid an oscillatory behavior of the system's response. All three inputs u_1, u_2, u_3 are saturated due to physical limitations of the motors:

$$\begin{aligned} -\overline{C}_{M_1} \leq \quad & u_1(t) \quad \leq \overline{C}_{M_1} \\ -\overline{C}_{M_2} \leq \quad & u_2(t) \quad \leq \overline{C}_{M_2} \\ 0 \leq \quad & u_3(t) \quad \leq \overline{F_T} \end{aligned} \tag{50}$$

Finally, the described controllers are implemented in discrete time with a sampling frequency of 100 Hz.

4.3. Simulation results and discussion

We simulate the take-off maneuver for three different aircrafts, whose effective areas matches those considered in section 3. The model and control parameters employed for the simulations are shown in Tables 4 and 5, respectively. In addition, the values $\rho = 1.2\,\mathrm{kg/m^3}$, $g = 9.81\,\mathrm{m/s^2}$ and the aerodynamic coefficients shown in Figure 13 have been used. The initial conditions (42) with $l_0 = 2\,\mathrm{m}$ and $x_{g,0} = 0$ were used for all three aircrafts. The number and size of the propellers, required to compute the related power according to equation (10), are the same as those considered in section 3, i.e. 2 propellers with efficiency 0.7 and 0.25 m, 0.5 m, 1 m of diameter, respectively, for the three aircraft sizes.

Examples of simulation results for the aircraft with $d = 10\,\mathrm{m}$ are shown in Figures 15-18. In Figure 15, it can be noted that the total travel distance of the slide is equal to 15 m, and that the aircraft starts the ascend after 12.4 m, i.e. when the take-off speed of 15.7 m/s has been reached. As shown in Figure 16, the motor M_2 exploits the full rated torque to accelerate and then to brake the slide, while M_1 employs a relatively small fraction of its available torque for the acceleration and then settles to a constant torque corresponding to the viscous friction at the aircraft's velocity. We

Table 4: System parameters employed to simulate the take-off maneuver.

d (m)	5	10	20
J_{M_1} (kg m^2)	1.3	30	490
β_{M_1} (kg/s)	0.001	0.002	0.003
r_{M_1} (m)	0.2	0.5	1
J_{M_2} (kg m^2)	0.03	0.1	2
β_{M_2} (kg/s)	0.001	0.002	0.003
r_{M_2} (m)	0.1	0.15	0.4
m_s (kg)	6	30	120
m (kg)	37.5	150	600
β_s (kg/s)	0.1	0.3	1
k_t (N/m)	$1\,10^5$	$9.1\,10^5$	$2.5\,10^5$
r_t (m)	0.0025	0.0075	0.0125
ρ_t (kg/m^3)	970	970	970
ω_β (rad/s^3)	10	10	10
ϑ_0 (rad)	0.24	0.24	0.24

Table 5: Control parameters employed to simulate the take-off maneuver.

d (m)	5	10	20
$\dot{x}_{g,to}$ (m/s)	30	30	30
$\dot{y}_{g,to}$ (m/s)	1	1	1
K_{M_1} (N m s/rad)	3	20	160
K_{M_2} (N m s/rad)	10	50	200
K_T (N m s/rad)	100	150	600
ω_p (rad/s)	16	32	32
$\omega_{z,1}$ (rad/s)	0.2	0.2	0.2
$\omega_{z,2}$ (rad/s)	1	2	2
$\overline{C}_{M_1}$ (N m)	750	3000	12000
$\overline{C}_{M_2}$ (N m)	48	290	3500
$\overline{F_T}$ (N)	80	350	600

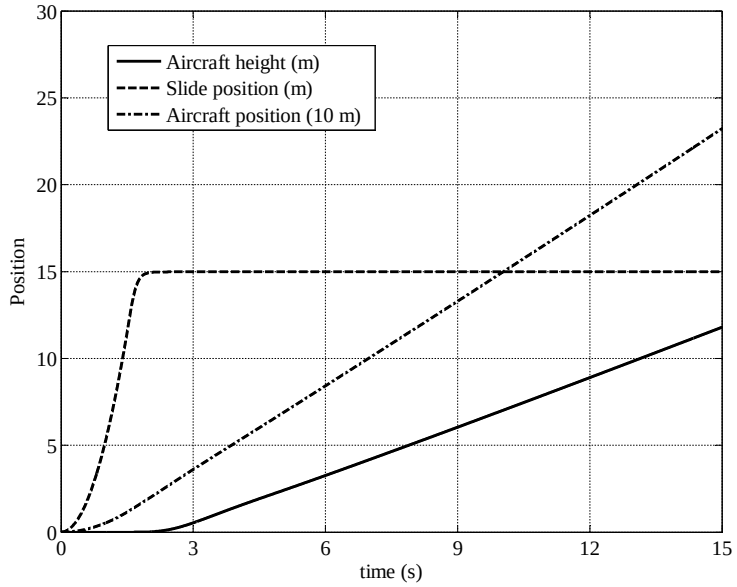

Figure 15: Simulation results with the 10-m-wingspan aircraft. Courses of the aircraft height, slide position and aircraft distance from the ground station (divided by 10 for the sake of clarity).

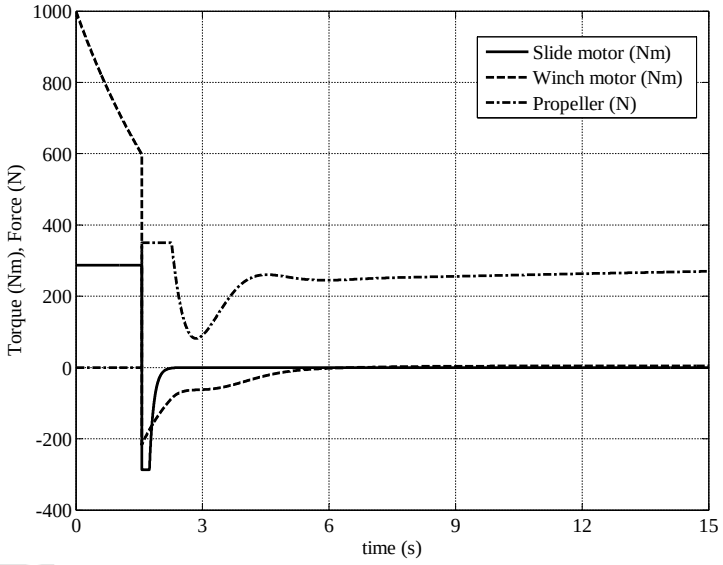

Figure 16: Simulation results with the 10-m-wingspan aircraft. Courses of the motor torques and of the propeller thrust.

remark that the power required to accelerate the drum, although substantial, does not give rise to additional costs, since the machine M_1 is already present and the power required for take-off is a small fraction of the one that occurs during power generation. The propeller is engaged only after take-off and, after a short transient, it settles to a steady value sufficient to achieve the desired vertical velocity. The behavior of the latter quantity as compared with its reference is reported in Figure 17. As shown in Figure 18, the peak power for the motors is reached at the instant when the aircraft

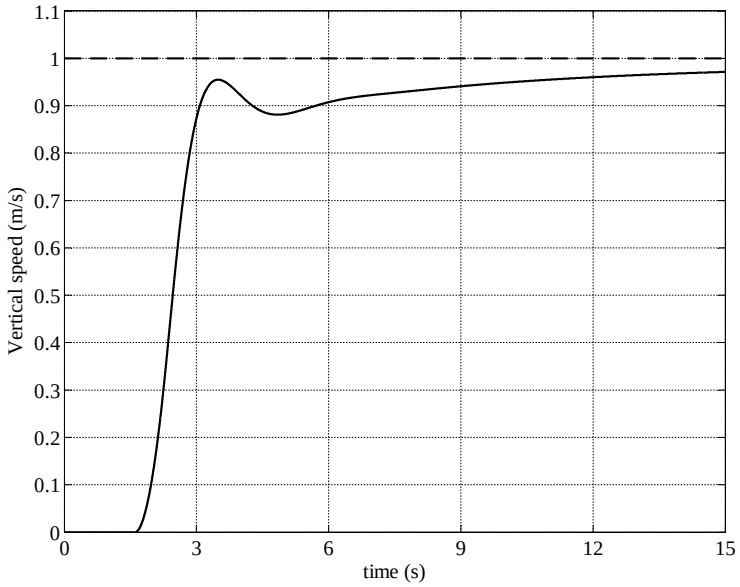

Figure 17: Simulation results with the 10-m-wingspan aircraft. Course of the vertical speed of the aircraft (solid) and the target value (dashed).

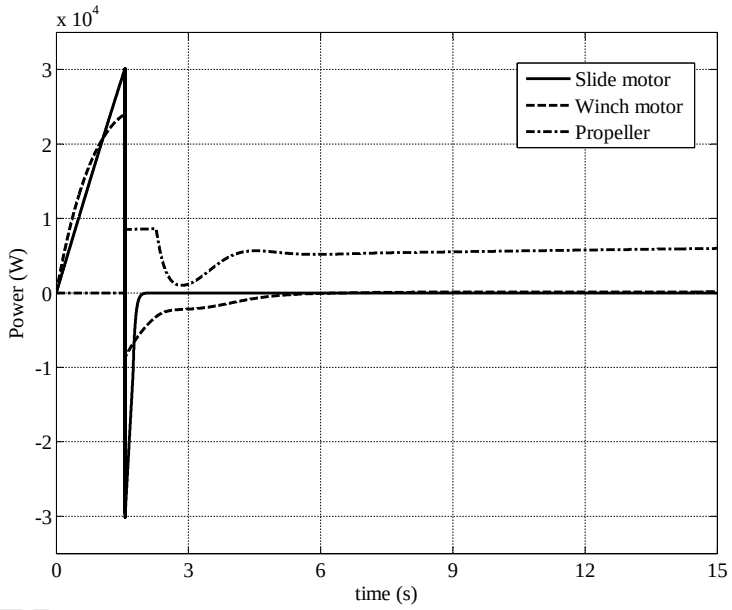

Figure 18: Simulation results with the 10-m wingspan aircraft. Courses of the motors' and propeller's power.

takes off. The results obtained with the other two aircrafts (d = 5 and 20 m) are qualitatively similar to those shown in Figures 15-18. In all cases, the total travel distance of the slide was about 15 m.

Table 6 shows a comparison between the power figures obtained from the simplified analysis of section 3 and those obtained with the simulations. The values of power required on the ground match very well, hence confirming the outcome of our simplified analysis. The larger simulated values for the required on-board power, with respect to the

Table 6: Comparison between the power values provided by the simplified equations and those provided by the numerical simulations. The percentages in brackets refer to the peak mechanical power of the generator with 15 m/s wind speed.

Wingspan (m)	5	10	20
Ground motor (kW) - simple equation	8 (11%)	31 (10%)	124 (10%)
Ground motor (kW) - simulation	8 (11%)	30 (10%)	140(11%)
Propeller (kW) - simple equation	2 (3%)	9 (3%)	37 (3%)
Propeller (kW) - simulation	3 (4%)	13 (4%)	50 (4%)

simplified analysis, are due to the inertia of the aircraft, which plays a role in the transient from zero vertical speed to the target one (see Figure 16), and due to its pitch, which has the effect of decreasing the thrust in horizontal direction and adding a braking contribution from the lift force projected onto the x_g-axis. Again, notwithstanding these effects, the on-board power required for the ascend appears to be a reasonable fraction of the system's power. Moreover, we did not optimize the design parameters or the controllers, which can still be adjusted in order to achieve different tradeoffs between peak power consumption and velocity of the transient from zero to the target vertical speed.

5. Conclusions

We presented an analysis of different concepts for the take-off phase of AWE systems based on rigid wings and ground-level power conversion, by means of basic equations. The derived equations can be used to evaluate the considered take-off approaches in a first approximation. Based on the equations and a set of reasonable system parameters, we concluded that a linear take-off maneuver with a ground acceleration phase and on-board propellers is the most promising approach from a techno-economic point of view. We refined the analysis of this maneuver by means of numerical simulations with a hybrid dynamical model. The simulation results predict slightly larger on-board power values than the simplified analysis, but they are still small compared to the total power of the generator. This indicates that the take-off equipment constitutes a rather small cost fraction of the total system costs. At the same time, the required land occupation appears to be reasonable. These outcomes confirm the technical and economic feasibility of this take-off technique. In recent experimental activities carried out at ABB Corporate Research, we could test the linear take-off approach with a small-scale demonstrator, obtaining peak on-ground and on-board power values that are consistent with those presented here, with a discrepancy in the range of 3-6% (see [26, 25] for details). We point out that the results obtained in this study depend on the design parameters given in Tables 1 and 2, which are typical values in the field of AWE.

Further studies will be devoted to a deeper analysis of the linear take-off approach and to the study of the landing approaches, both with finer dynamical models, also accounting for wind turbulence, and with experimental activities.

[1] U. Ahrens, M. Diehl, and R. Schmehl, editors. *Airborne Wind Energy*. Green Energy and Technology. Springer-Verlag Berlin, 2014.

[2] C.L. Archer. *Airborne Wind Energy*, chapter 5. An Introduction to Meteorology for Airborne Wind Energy, page 81. Green Energy and Technology. Springer-Verlag, Berlin, 2014.

[3] C.L. Archer and K. Caldeira. Global assessment of high-altitude wind power. *Energies*, 2(2):307–319, 2009.

[4] I. Argatov, P. Rautakorpi, and R. Silvennoinen. Estimation of the mechanical energy output of the kite wind generator. *Renewable Energy*, 34:1525, 2009.

[5] I. Argatov and R. Silvennoinen. Energy conversion efficiency of the pumping kite wind generator. *Renewable Energy*, 35:1052, 2010.

[6] J. H. Baayen and W. J. Ockels. Tracking control with adaption of kites. *IET Control Theory and Applications*, 6(2):182–191, 2012.

[7] Eelke Bontekoe. Up! - how to launch and retrieve a tethered aircraft. Master's thesis, TU Delft, August 2010. Accessed in August 2015 at http://repository.tudelft.nl/.

[8] A. Bormann, M. Ranneberg, P. Kövesdi, C. Gebhardt, and S. Skutnik. *Airborne Wind Energy*, chapter 24. Development of a Three-Line Ground-Actuated Airborne Wind Energy Converter, page 427. Green Energy and Technology. Springer-Verlag, Berlin, 2014.

[9] A. Bosch, R. Schmehl, P. Tiso, and D. Rixen. *Airborne Wind Energy*, chapter 17. Nonlinear Aeroelasticity, Flight Dynamics and Control of a Flexible Membrane Traction Kite, page 307. Green Energy and Technology. Springer-Verlag, Berlin, 2014.

[10] A. Bosch, R. Schmehl, P. Tiso, and D. Rixen. Dynamic nonlinear aeroelastic model of a kite for power generation. *AIAA Journal of Guidance, Control and Dynamics*, 37(5):1426–1436, 2014.

[11] J. Breukels, R. Schmehl, and W. Ockels. *Airborne Wind Energy*, chapter 16. Aeroelastic Simulation of Flexible Membrane Wings based on Multibody System Dynamics, page 287. Green Energy and Technology. Springer-Verlag, Berlin, 2014.

[12] M. Canale, L. Fagiano, and M. Milanese. High altitude wind energy generation using controlled power kites. *IEEE Transactions on Control Systems Technology*, 18(2):279 –293, mar. 2010.

[13] M.R. Doyle, D.J. Samuel, T. Conway, and R.R. Klimowski. Electromagnetic aircraft launch system-EMALS. *IEEE Transactions on Magnetics*, 31(1):528 –533, 1995.

[14] Michael Erhard and Hans Strauch. Flight control of tethered kites in autonomous pumping cycles for airborne wind energy. *Control Engineering Practice, submitted. preprint available on arXiv:1409.3083*.

[15] Michael Erhard and Hans Strauch. Control of towing kites for seagoing vessels. *IEEE Transactions on Control Systems Technology*, 21(5):1629 – 1640, 2013.

[16] J. Gibson. Understanding the winch launch. *Sailplane and Gliding*, 38(1):28 – 31, 1987.

[17] R. H. Luchsinger F. Gohl. *Airborne Wind Energy*, chapter 18. Simulation Based Wing Design for Kite Power, page 325. Green Energy and Technology. Springer-Verlag, Berlin, 2014.

[18] L. Fagiano, K. Huynh, B. Bamieh, and M. Khammash. On sensor fusion for airborne wind energy systems. *IEEE Transactions on Control Systems Technology*, 22(3):930–943, 2014.

[19] L. Fagiano and T. Marks. Design of a small-scale prototype for research in airborne wind energy. *IEEE/ASME Transactions on Mechatronics*, 20(1):166–177, 2014.

[20] L. Fagiano and M. Milanese. Airborne wind energy: an overview. In *American Control Conference 2012*, pages 3132–3143, Montreal, Canada, 2012.

[21] L. Fagiano, M. Milanese, and D. Piga. High-altitude wind power generation. *IEEE Transactions on Energy Conversion*, 25(1):168 –180, mar. 2010.

[22] L. Fagiano, M. Milanese, and D. Piga. Optimization of airborne wind energy generators. *International Journal of Robust and Nonlinear Controll*, 2011. In press, early view available. doi: 10.1002/rnc.1808.

[23] L. Fagiano, A.U. Zgraggen, M. Morari, and M. Khammash. Automatic crosswind flight of tethered wings for airborne wind energy: modeling, control design and experimental results. *IEEE Transactions on Control Systems Technology*, 22(4):1433–1447, 2014.

[24] Lorenzo Fagiano, Eric Nguyen-Van, Felix Rager, Stephan Schnez, and Christian Ohler. Autonomous tethered take-off and flight for airborne wind energy - movie. YouTube: https://www.youtube.com/watch?v=UPiTiHPXciE, March 2016.

[25] Lorenzo Fagiano, Eric Nguyen-Van, Felix Rager, Stephan Schnez, and Christian Ohler. Autonomous take off and flight of a tethered aircraft for airborne wind energy. *Submitted. Preliminary version available on ArXiv e-prints: 1608.01889*, http://arxiv.org/abs/1608.01889, 2016, submitted.

[26] Lorenzo Fagiano, Eric Nguyen-Van, Felix Rager, Stephan Schnez, and Christian Ohler. A small-scale prototype to study the take-off of tethered rigid aircrafts for airborne wind energy. *Submitted. Preliminary version available on ArXiv e-prints: 1608.01846*, http://arxiv.org/abs/1608.01846, 2016, submitted.

[27] U. Fechner and R. Schmehl. Feed-forward control of kite power systems. *Journal of Physics: Conference Series*, 524:012081, 2014.

[28] F. Fritz. *Airborne Wind Energy*, chapter 20. Application of an Automated Kite System for Ship Propulsion and Power Generation, page 359. Green Energy and Technology. Springer-Verlag, Berlin, 2014.

[29] T. Håarklau. Kitemill, a Driver of Second-Generation Wind Energy! Oral presentation at The International Airborne Wind Energy Conference 2015, available online: https://collegerama.tudelft.nl/Mediasite/Play/6ef7e15c6c0c418bb24ca8f6b3d79c0c1d (last accessed 11 December 2016).

[30] J. H. Horlock. *Actuator Disk Theory: Discontinuities in Thermo Fluid Dynamics*. McGraw-Hill, 1978.

[31] B. Houska and M. Diehl. Optimal control for power generating kites. In *9th European Control Conference*, pages 3560–3567, Kos, GR, 2007.

[32] David G. Hull. *Fundamentals of Airplane Flight Dynamics*. Springer-Verlag, Berlin, 2007.

[33] M. Kruijff. Preparing for a commercially viable awe system in the utility sector. Oral presentation at The International Airborne Wind Energy Conference 2015, available online: https://collegerama.tudelft.nl/Mediasite/Play/2e1f967767d541b1b1f2c912e8eff7df1d (last accessed 21 September 2016).

[34] R. Leloup, K. Roncin, G. Bles, J.B. Leroux, C. Jochum, and Y. Parlier. *Airborne Wind Energy*, chapter 19. Estimation of the Lift-to-Drag Ratio Using the Lifting Line Method: Application to a Leading Edge Inflatable Kite, page 339. Green Energy and Technology. Springer-Verlag, Berlin, 2014.

[35] D. Vander Lind. *Airborne Wind Energy*, chapter 28. Analysis and Flight Test Validation of High Performance Airborne Wind Turbines, page 473. Green Energy and Technology. Springer-Verlag, Berlin, 2014.

[36] M. L. Loyd. Crosswind kite power. *Journal of Energy*, 4(3):106–111, 1980.

[37] R. Luchsinger. Closing the gap: Pumping cycle kite power with twings. Oral presentation at The International Airborne Wind Energy Conference 2015, available online: https://collegerama.tudelft.nl/Mediasite/Play/646b794e7ac54320ba48ba9f41b41f811d (last accessed 21 September 2016).

[38] Makani Power Inc. http://www.makanipower.com.

[39] M. S. Manalis. Airborne windmills and communication aerostats. *Journal of Aircraft*, 13(7):543–544, 1976.

[40] Barnes W. Mccormick. *Aerodynamics, Aeronautics, and Flight Mechanics*. John Wiley and Sons, 1995.

[41] M. Milanese, F. Taddei, and S. Milanese. *Airborne Wind Energy*, chapter 21. Design and Testing of a 60 kW Yo-Yo Airborne Wind Energy Generator, page 373. Green Energy and Technology. Springer-Verlag, Berlin, 2014.

[42] R. Ruiterkamp and Sören Sieberling. *Airborne Wind Energy*, chapter 26. Description and Preliminary Test Results of a Six Degrees of Freedom Rigid Wing Pumping System, page 443. Green Energy and Technology. Springer-Verlag, Berlin, 2014.

[43] J. Stuyts, G. Horn, W. Vandermeulen, J. Driesen, and M. Diehl. Effect of the electrical energy conversion on optimal cycles for pumping airborne wind energy. *IEEE Transactions on Sustainable Energy*, 6(1):2–10, 2015.

[44] R. van der Vlugt, J. Peschel, and R. Schmehl. *Airborne Wind Energy*, chapter 23. Design and Experimental Characterization of a Pumping Kite Power System, page 403. Green Energy and Technology. Springer-Verlag, Berlin, 2014.

[45] C. Vermillion, B. Glass, and A. Rein. *Airborne Wind Energy*, chapter 30. Lighter-Than-Air Wind Energy Systems, page 501. Green Energy and Technology. Springer-Verlag, Berlin, 2014.

[46] M. Zanon, S. Gros, and M. Diehl. Rotational start-up of tethered airplanes based on nonlinear mpc and mhe. In *European Control Conference (ECC) 2013*, pages 1023–1028, Zuerich, Switzerland, July 2013, 2013.

[47] M. Zanon, S. Gros, and M Diehl. *Airborne Wind Energy*, chapter 12. Model Predictive Control of Rigid-Airfoil Airborne Wind Energy Systems, page 219. Green Energy and Technology. Springer-Verlag, Berlin, 2014.

[48] A.U. Zgraggen, L. Fagiano, and M. Morari. Real-time optimization and adaptation of the crosswind flight of tethered wings for airborne wind energy. *IEEE Transactions on Control Systems Technology*, 23(2):434–448, 2015.

[49] U. Zillmann and S. Hach. *Airborne Wind Energy*, chapter 7. Financing Strategies for Airborne Wind Energy, page 117. Green Energy and Technology. Springer-Verlag, Berlin, 2014.

Paper title: On the Take-off of Airborne Wind Energy Systems Based on Rigid Wings

Authors: Lorenzo Fagiano and Stephan Schnez

Highlights

- An assessment of four take-off approaches for airborne wind energy is presented.
- The power required for the take-off functionality is related to the overall generated power.
- A theoretical analysis shows that a linear take-off concept is the most viable one.
- Numerical simulations refine the theoretical results and further confirm the main findings.